ARTICLE　OPEN

Check for updates

Revisiting the specificity and ability of phospho-S129 antibodies to capture alpha-synuclein biochemical and pathological diversity

Hilal A. Lashuel [1,5 ✉], Anne-Laure Mahul-Mellier [1,5], Salvatore Novello [1,5], Ramanath Narayana Hegde[1], Yllza Jasiqi[1], Melek Firat Altay[1], Sonia Donzelli[1], Sean M. DeGuire[1], Ritwik Burai[1], Pedro Magalhães [1], Anass Chiki[1], Jonathan Ricci [1], Manel Boussouf[1], Ahmed Sadek[1], Erik Stoops[2], Christian Iseli [3,4] and Nicolas Guex [3,4]

Antibodies against phosphorylated alpha-synuclein (aSyn) at S129 have emerged as the primary tools to investigate, monitor, and quantify aSyn pathology in the brain and peripheral tissues of patients with Parkinson's disease and other neurodegenerative diseases. Herein, we demonstrate that the co-occurrence of multiple pathology-associated C-terminal post-translational modifications (PTMs) (e.g., phosphorylation at Tyrosine 125 or truncation at residue 133 or 135) differentially influences the detection of pS129-aSyn species by pS129-aSyn antibodies. These observations prompted us to systematically reassess the specificity of the most commonly used pS129 antibodies against monomeric and aggregated forms of pS129-aSyn in mouse brain slices, primary neurons, mammalian cells and seeding models of aSyn pathology formation. We identified two antibodies that are insensitive to pS129 neighboring PTMs. Although most pS129 antibodies showed good performance in detecting aSyn aggregates in cells, neurons and mouse brain tissue containing abundant aSyn pathology, they also showed cross-reactivity towards other proteins and often detected non-specific low and high molecular weight bands in aSyn knock-out samples that could be easily mistaken for monomeric or high molecular weight aSyn species. Our observations suggest that not all pS129 antibodies capture the biochemical and morphological diversity of aSyn pathology, and all should be used with the appropriate protein standards and controls when investigating aSyn under physiological conditions. Finally, our work underscores the need for more pS129 antibodies that are not sensitive to neighboring PTMs and more thorough characterization and validation of existing and new antibodies.
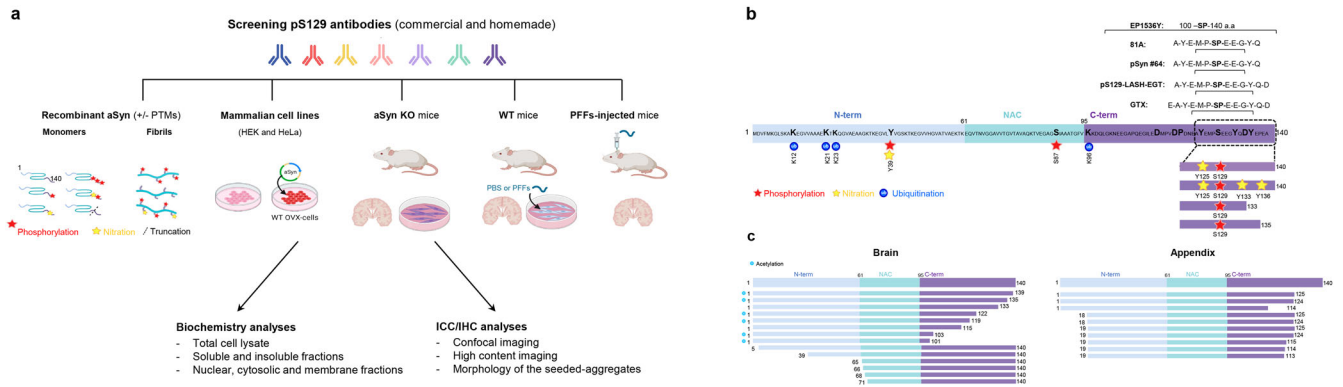
INTRODUCTION

Phosphorylation of alpha-synuclein (aSyn) at serine 129 (pS129) has become the most commonly used marker of aSyn pathology formation and propagation in Parkinson's disease (PD) and other synucleinopathies. Initial studies suggested that the majority (>90%) of aSyn in PD and dementia with Lewy bodies (DLB) brains is phosphorylated at S129[1]. Subsequent studies on the biochemical composition of Lewy bodies (LB) revealed that pS129 is the dominant aSyn post-translational modification (PTM) in LB[2,3]. Furthermore, an increase in pS129 levels in both cellular models and brains of animal models of synucleinopathies is usually associated with the appearance of aSyn aggregates, and the majority of pS129-aSyn species are typically found in the insoluble fractions of brains and cell extracts[4]. Finally, pS129 immunoreactivity has been observed in peripheral tissues and organs associated with non-motor symptoms of PD. These observations, combined with the development of a large number of antibodies against pS129-aSyn, have led to an increased reliance on pS129 antibodies as the primary tools for monitoring and quantifying aSyn pathology formation and spreading in human brains, peripheral tissues, and in cellular and animal models of synucleinopathies[5].

This has prompted several studies to assess the sensitivity and specificity of pS129-aSyn antibodies. However, most of these studies have focused primarily on the cross-reactivity of the pS129-aSyn antibodies with other proteins[4,6,7]. Rutherford et al. reported that some of their in-house generated monoclonal pS129 antibodies cross-reacted with neurofilament subunits (NFL) phosphorylated at Serine 473 while others cross-reacted with other proteins[8]. Several pS129 antibodies have also been shown to cross-react with cellular nuclei under conditions where aSyn is either not expressed or could not be detected in nuclear fractions by Western blotting (WB)[9,10]. Delic et al. compared the specificity of four of the most commonly used pS129 monoclonal antibodies (clones EP1536Y, MJF-R13, 81A, and pSyn#64) in brain slices and protein lysates from mice and rats[4]. Three of the four clones (MJF-R13, 81 A, and pSyn#64) showed non-specific staining in tissues from aSyn knock-out (KO) mice and all four antibodies cross-reacted with other proteins. Consistent with previous studies by Rutherford et al. EP1536Y showed the highest sensitivity and specificity for detecting pS129-aSyn[4,9]. However, in a recent study Arlinghaus et al. evaluated the specificity of MJF-R13, pSyn#64, and EP1536Y, and reported that all three showed cross-reactivity and lack of specificity towards endogenous aSyn in wildtype (WT) or *SNCA* KO brain slices or primary cultures [by immunohistochemistry (IHC) or immunocytochemistry (ICC)][11]. Recently, Fayyad et al. described the generation of three novel pS129-aSyn antibodies[5]. However, the specificity and affinity of these antibodies were assessed only against unmodified WT

[1]Laboratory of Molecular and Chemical Biology of Neurodegeneration, School of Life Sciences, Brain Mind Institute, Ecole Polytechnique Fédérale de Lausanne (EPFL), 1015 Lausanne, Switzerland. [2]ADx NeuroSciences, Technologiepark 94, Ghent, Belgium. [3]Bioinformatics Competence Center, Ecole Polytechnique Fédérale de Lausanne, 1015 Lausanne, Switzerland. [4]Bioinformatics Competence Center, University of Lausanne, 1015 Lausanne, Switzerland. [5]These authors contributed equally: Hilal A. Lashuel, Anne-Laure Mahul-Mellier, Salvatore Novello. ✉email: hilal.lashuel@epfl.ch

Fig. 1 Assessment of the background and specificity of commercial and homemade pS129 antibodies in vitro and in cellular and animal models. a The diagram depicts the workflow of our study to assess the background and specificity of commercial and homemade pS129 antibodies using recombinant aSyn monomers and fibrils (WT or carrying specific PTMs such as nitration, phosphorylation and/or truncation), mammalian cell lines overexpressing aSyn, aSyn KO primary neurons, WT neurons treated with aSyn PFFs or WT mice injected with aSyn PFFs. The background and specificity of the selected pS129 antibodies were evaluated by Western blot analyses or ICC or HTS combined with confocal imaging. Panel A was created using BioRender.com. **b** The diagram depicts aSyn human sequence, the epitopes of each of the pS129 antibodies (whenever available), and the post-translational modifications that can occur concomitantly in the C-terminal region of aSyn. **c** The diagram depicts truncations that occurs in the different regions of aSyn in human brains and the appendix.

recombinant aSyn and unpurified in vitro Polo-Like Kinase 2 (PLK2) phosphorylated pS129-aSyn standards[5]. Interestingly, most of the antibodies reported in the study by Fayyad et al. seem to detect primarily aSyn monomeric bands and did not detect the classical pattern of high molecular weight (HMW) aSyn bands usually detected in the insoluble fractions from PD brain homogenates[5]. This increasing reliance on pS129 antibodies necessitates the development of robust standardized pipelines for the characterization and validation of these antibodies before their use in PD and neurodegenerative disease research.

Increasing evidence from the biochemical characterization of aSyn pathology isolated from brain, peripheral tissues, and biological fluids by mass spectrometry show that aSyn is subjected to several modifications in the vicinity of Serine 129, including phosphorylation at Tyrosine 125 (Y125)[12], nitration at Y125, Y133, and Y136[13] and truncations at residues 119, 122, 133 and 136[1,3,14,15]. Both aSyn phosphorylated at S129 and Y125 were found in pathological aggregates from the same brain tissue of a G51D case[16] (Fig. 1a). For example, several IHC studies examining the distribution of aSyn species in pathological aggregates have demonstrated that they are enriched in phosphorylated, and C-terminally truncated aSyn species[3,14,17–21]. Recent mass spectrometry studies on LBs and insoluble brain-derived aSyn aggregates have identified several truncated aSyn species, including aSyn proteins that are truncated at both N- and C-terminal regions (Fig. 1c)[1,14,15,22]. In the appendix, aSyn was predominantly a mixture of different species truncated at the N-terminus, C-terminus, or both termini. Thus far, all the studies on mapping aSyn PTMs have focused on identifying or characterizing one PTM at a time and global mapping of the distribution of aSyn species in biological samples rather than the distribution of PTMs that co-occur at the single-molecule level.

We hypothesized that the presence of multiple PTMs in the C-terminus could significantly influence or mask the detection of pS129-aSyn[1,3,16,23–25]. To test this hypothesis, we systematically assessed, the effect of the co-occurrence of pathology-associated C-terminal PTMs on the detection of pS129-aSyn. This was achieved by leveraging our protein synthesis and recombinant expression platforms, which enabled the generation of a library of highly pure and site-specifically modified recombinant and semisynthetic full-length aSyn proteins phosphorylated at S129 and bearing different combinations of other disease-associated PTMs, including Tyrosine 125 phosphorylation/nitration and C-terminal truncations at 133 and 135 (Fig. 1b). However, given

the large number of available pS129 antibodies, it was not possible to assess them all. Therefore, for this study, we conducted a thorough review of the aSyn literature and selected the five most commonly used commercially available antibodies across different methods. These include two mouse monoclonal antibodies (pSyn#64 and 81A) and two monoclonal rabbit antibodies: EP1536Y, MJF-R13 and the polyclonal rabbit GTX) (Supplementary Fig. 1). In addition, we included a homemade polyclonal rabbit antibody (pS129-LASH-EGT) (Fig. 1b). While working with these antibodies, we observed, as reported previously[4,9,26], that they cross-react with other proteins and that some of the undefined signals could be easily mistaken for aSyn signals. This prompted us to expand the pipeline for assessing the specificity of pS129 antibodies to include mouse brain tissues, in primary neurons and mammalian cells lacking or expressing aSyn. Furthermore, we investigated the differential ability of these antibodies to capture the diversity of aSyn aggregates in neuronal and in vivo models of aSyn seeding and pathology spreading. Our results show that several C-terminal PTMs found in aSyn pathological aggregates eliminate or mask the detection of pathological aggregates by pS129 antibodies. These observations suggest some pS129 antibodies cannot capture the biochemical diversity of pathological aSyn species, and their use might result in underestimating aSyn pathology or selective preference for pathological aggregates composed of the full-length aSyn protein. This is important because recent studies from our group have identified one type of aSyn inclusions, astroglial synuclein accumulations, that are composed solely of aSyn proteins where the first 30 N-terminal amino acids and last 35-40 C-terminal amino acids are absent. Such aSyn accumulations are not detected by any C-terminal targeting antibodies, including pS129 antibodies.

Furthermore, we demonstrate that these antibodies exhibit differential cross-reactivity towards a large number of proteins of various sizes and subcellular localization, in particular under conditions of basal expression of aSyn or in the absence of abundant aSyn pathology. Finally, we searched the human and mouse proteome and generated a comprehensive list of candidate proteins that could cross-react with pS129 antibodies. Taken together, our findings underscore the critical importance of developing more specific pS129 antibodies, exercising caution in interpreting results from experiments relying mainly on the use of pS129 antibodies, and including the appropriate controls in experiments using these antibodies to investigate aSyn biology or mechanisms of pathology formation and spreading. Specific
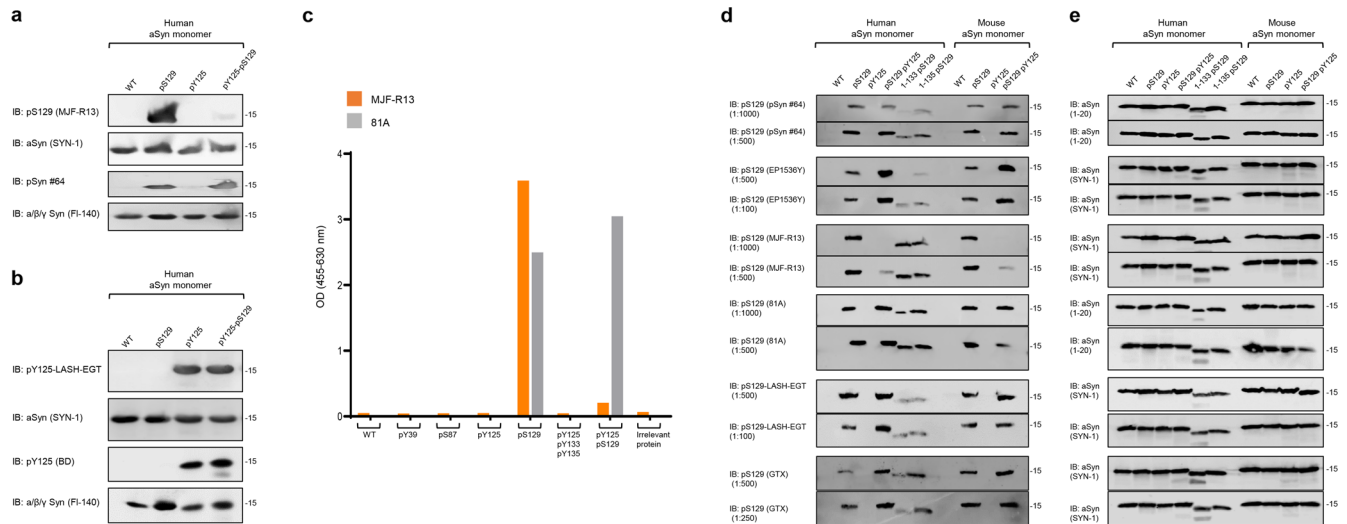
Fig. 2 PTMs nearby S129 residue interferes with the capacity of some pS129 antibodies to detect pS129-aSyn. The capacity of human or mouse recombinant monomeric aSyn (WT or modified by specific PTMs) to be detected by pS129 commercial antibodies (pSyn#64, MJF-R13, 81A, EP1536Y, and GTX) or the LASH-EGT homemade pS129 antibody was assessed by WB (**a**, **b**, **d**) or ELISA (**c**). **a**, **b** Forty nanograms of human recombinant monomeric aSyn unphosphorylated (WT) or phosphorylated at the S129 residue (pS129) or di-phosphorylated (pY125/pS129) were detected by WB using total aSyn antibodies (SYN-1 or FI-140 α/β/γ synuclein) combined with either **a** commercial (MJF-R13 or pSyn#64) and homemade (LASH-EGT) pS129 antibodies or **b** commercial pY125 antibody (BD) or the homemade antibody LASH-EGT-pY125. **c** ELISA confirmed that MJF-R13, but not 81A, is no longer able to detect pS129-aSyn when aSyn was di-phosphorylated (pY125/pS129). **d**, **e** One-hundred nanograms of unmodified aSyn (WT) or phosphorylated aSyn at S129 and/or Y125 residues (respectively named pS129, pY125 or pS129/pY125) full length or truncated after residues 133 (1-133/pS129) or 135 (1-135/pS129) were detected by WB using pS129 antibodies (**d**) or total aSyn antibodies (SYN-1 or LASH-EGT 1-20) (**e**). All blots were derived from the same experiment and were processed in parallel.

recommendations for developing, validating, and characterizing aSyn antibodies are presented and discussed.

RESULTS

All pS129 antibodies tested robustly detected phosphorylated aSyn (pS129), but not the unmodified protein

As the first step in our study, we assessed the specificity of the pS129 antibodies (Supplementary Fig. 3B) against highly pure aSyn protein that is site-specifically phosphorylated at S129 only and unmodified WT aSyn (Supplementary Fig. 2). While pSyn#64, EP1536Y, MJF-R13, 81A, GTX were unable to detect the unmodified protein and showed robust signals for pS129-aSyn, the homemade pS129-LASH-EGT had a low recognition of non-phosphorylated aSyn (Supplementary Fig. 4A). Next, we assessed the specificity of three pS129 antibodies (pSyn#64, MJF-R13 and pS129-LASH-EGT) against aSyn proteins that are site-specifically phosphorylated at residue Y125 (Fig. 2a and Supplementary Fig. 2A, B) or other residues such as Y39 or S87 (Supplementary Fig. 4B, C). None of the pS129 antibodies tested could detect any phosphorylated aSyn where S129 was not phosphorylated. These findings demonstrate that the selected pS129 antibodies are highly specific for pS129.

The presence of additional PTMs close to the S129 interfere with the detection of pS129

The majority of pS129 antibodies were developed based on the assumption that neighboring modifications either do not co-occur with pS129 or do not influence its detection. Therefore, most peptide antigens used to raise antibodies were comprised of 3–6 residues on each side of S129 (Fig. 1b and Supplementary Fig. 3B) and were modified only at S129. We hypothesized that the co-occurrence of pS129 and other PTMs in the C-terminal region spanning residues 123–135 could interfere with pS129 detection. To test this hypothesis, we first assessed whether phosphorylation of tyrosine 125 (Y125), which has been observed in pS129 immunoreactive LBs[16], could influence the detection of pS129. Towards this goal, we generated semi-synthetic human full-length aSyn proteins site-specifically phosphorylated on residue S129 (pS129) or residue Y125 (pY125) or di-phosphorylated (pY125/pS129) (Supplementary Fig. 2C). The proteins were produced as described previously[27–29].

Initially, we assessed the ability of two of the most commonly used pS129 antibodies (MJF-R13 and pSyn#64) to detect singly (pS129) and diphosphorylated aSyn pY125/pS129 by WB. To our surprise, the MJF-R13 detected only singly phosphorylated pS129, whereas the pSyn#64 antibody detected both singly pS129 and di-phosphorylated pY125/pS129-aSyn proteins (Fig. 2a, b). Interestingly, the two pY125 antibodies tested detected both pY125 and pY125/pS129-aSyn (Fig. 2b). These findings confirmed our hypothesis and suggested that the presence of other C-terminal PTMs, e.g., pY125, could interfere with the detection of pS129 by some antibodies raised against this PTM. However, pS129 does not seem to influence the detection of pY125. These findings were validated using an enzyme-linked immunosorbent assay (ELISA) where two pS129 antibodies (MJF-R13 and 81A) were evaluated using a library of aSyn proteins containing single (pY39, pS87, pY125, pS129) or multiple C-terminal phosphorylation sites (pY125/pS129 and pY125/pY133/pY136). As shown in Fig. 2c, none of the pS129 antibodies detected aSyn proteins phosphorylated at other residues (pY39, pS87, pS129), and only the 81A antibody detected aSyn that is phosphorylated at both pY125 and pS129. These observations prompted us to conduct a more systematic investigation of the impact of other disease-associated PTMs on the detection of phosphorylated aSyn by pS129 antibodies (Fig. 2c).

Several studies have confirmed that some of the aSyn found in LBs in human brain tissue is truncated at several residues, including Tyrosine 133 (Y133) or Aspartic acid 135 (D135)[1,15,30] (Fig. 1c). Recent studies have also reported that aSyn is cleaved at Y125, S129, Y133, and D135 in preformed fibrils (PFFs) seeded neuroblastoma cell lines[31]. Similarly, we and others have shown that human and mouse aSyn PFFs undergo multiple C-terminal
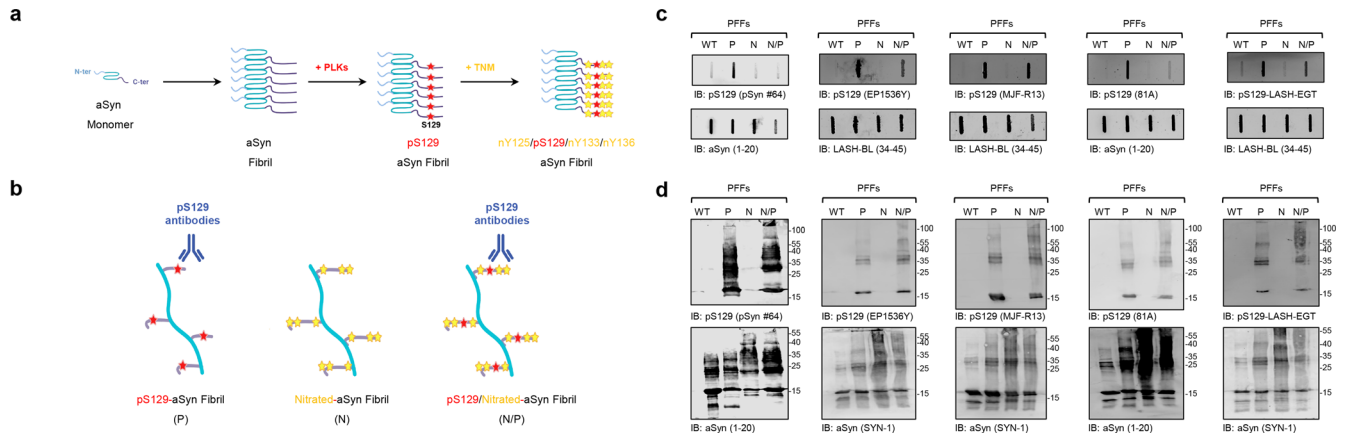
Fig. 3 Nitration of aSyn does not impair the capacity of pS129 antibodies to detect pS129 fibrils. a Preparation of aSyn fibrils carrying both phosphorylation and nitration modifications. aSyn fibrils were first site-specifically phosphorylated at S129 residue by being incubated with PLK3. Afterwards, TNM was added to induce the nitration of the phosphorylated aSyn fibrils. **b** The capacity of aSyn fibrils site-specifically phosphorylated at S129 and/or nitrated to be detected by the pS129 commercial antibodies (pSyn#64, MJF-R13, 81A, and EP1536Y) or the LASH-EGT homemade pS129 antibody was assessed by slot blot (**c**) and WB (**d**) analyses. **a, b** were created using BioRender.com. **c, d** Thirty-six nanograms of aSyn fibrils (PFFs) that were unmodified (WT), phosphorylated (P), nitrated (N), or nitrated/phosphorylated (N/P) were detected by slot blot (**c**) and WB (**d**) using pS129 antibodies (top panel) in combination with total aSyn antibodies (1–20 and 34–45, bottom panel). All blots were derived from the same experiment and were processed in parallel.

cleavages, including E114, D115, D119, D121, S122, Y125, and D135[31,32]. Therefore, we sought to assess the ability of the pS129 antibodies to detect aSyn species that are both phosphorylated at S129 and truncated at the far C-terminus, at residues 133 or 135. To produce aSyn bearing both modifications, monomeric full-length or truncated (1–133 or 1–135) aSyn were phosphorylated specifically at S129 using the Polo-Like Kinase 3 (PLK3) in vitro as previously described[28,29]. The homogeneously phosphorylated proteins were purified by RP-HPLC, and the final purity of the proteins was confirmed by sodium dodecyl sulfate–polyacrylamide gel electrophoresis (SDS-PAGE), ultra-performance liquid chromatography (UPLC), and liquid chromatography–mass spectrometry (LC-MS) analyses (Supplementary Fig. 2D). With all these proteins in hand, we screened by WB the five most commonly used pS129 antibodies in the PD field (pSyn#64, MJF-R13, 81A, EP1536Y, and GTX, Supplementary Fig. 1), in addition to our pS129 homemade antibody (pS129-LASH-EGT).

As shown in Fig. 2d, e, all six antibodies evaluated in this study detected the singly phosphorylated (pS129) but not the unmodified human and mouse aSyn proteins. Interestingly, the aSyn proteins bearing pS129 and truncations at 133 or 135 were barely detected by three (pSyn#64, EP1536Y, and pS129-LASH-EGT) out of the six antibodies (Fig. 2d, e). Detection of pS129 by MJF-R13 and 81A was not affected by truncation at 133 or 135, whereas the GTX antibody detected 1-135/pS129 but not 1-133/pS129-aSyn. This data confirmed that cleavages in the sequences flanking S129 residue (e.g., truncations at 114, 119, 115, 120, 121, 129, 133, or 135)[1,3,14,18,32] could either abolish (e.g., truncations at 114, 119, 120 or 121) or interfere with (e.g., truncations at 129, 133 or 135) pS129 detection by all or some pS129 antibodies, respectively. Among the six antibodies tested, only MJF-R13 completely lost its ability to detect di-phosphorylated human and mouse aSyn at S129 and Y125 (pY125/pS129) while efficiently detecting the singly phosphorylated aSyn at S129 or 1-133/pS129-aSyn and 1-135/pS129-aSyn (Fig. 2d). The EP1536Y antibody detected di-phosphorylated (pY125/pS129) aSyn (human and mouse) but failed to detect pS129-aSyn truncated after residues 133 or 135. Overall, only the 81A clone was insensitive to neighboring PTMs and detected pS129-aSyn that is also phosphorylated at Y125 or truncated at residue 133 or 135 (Fig. 2d). Together, these results show that the co-occurrence of pS129 and other C-terminal modifications interfere with pS129-aSyn detection but show that it is possible

to develop antibodies capable of capturing the biochemical diversity of pS129-aSyn species in vitro.

Not all pS129 antibodies detect aSyn fibrils that are subjected to both C-terminal nitration (Y125/Y133/Y136) and phosphorylation (S129)

Given that C-terminal aSyn PTMs are more abundant in the aggregated state of aSyn, we next sought to determine if neighboring modifications could influence the detection of aSyn fibrils phosphorylated at S129. We first generated aSyn fibrils site-specifically phosphorylated at S129 (Fig. 3a). This was achieved by in vitro phosphorylation of aSyn PFFs using PLK3 (Supplementary Fig. 2C). Next, fibrils nitrated at all tyrosine residues (nY39/nY125/nY133/nY136) were also generated by chemical nitration of fibrils using Tetranitromethane (TNM), as described previously[33] (Supplementary Fig. 5). Finally, fibrils that were both phosphorylated and nitrated (pS129/nY125/nY133/nY136) were also generated by treatment of pS129-aSyn fibrils with TNM (Supplementary Fig. 5). In all cases, the extent of fibril modification was verified by mass spectrometry (Supplementary Fig. 5A).

The pS129 antibodies pSyn#64, EP1536Y, MFJ-R13, 81 A, and LASH-EGT, were then screened by dot blot and WB using pS129-aSyn monomers, pS129-aSyn fibrils, and unmodified aSyn fibrils as a negative control. As shown in Fig. 3b, c, all five antibodies detected pS129-aSyn fibrils, but not the unmodified aSyn fibrils. Nitration of the three C-terminal tyrosine residues abolished the ability of the pSyn#64 and 81A antibodies to detect pS129 in pS129/nY125/nY133/nY136-aSyn (Fig. 3b, c). In contrast, these modifications did not significantly affect the detection using MJF-R13 and LASH-EGT. The EP1536Y antibody showed reduced signal for pS129/nY125/nY133/nY136-aSyn fibrils compared to pS129-aSyn fibrils. These findings demonstrate that some pS129 antibodies may fail to capture aSyn fibrils that are both phosphorylated and nitrated at the C-terminal domain of the protein. Interestingly, all five antibodies showed high specificity and immunoreactivity towards both monomeric and high molecular weight bands of both pS129/nY125/nY133/nY136-aSyn fibrils and pS129-aSyn fibrils in denaturing conditions (WB analyses) (Fig. 3c). These results suggest that treatment with denaturing agents helps reveal the pS129 signal masked by the presence of some neighboring PTMs, e.g., nitration. They also demonstrate that antibodies that were not affected by
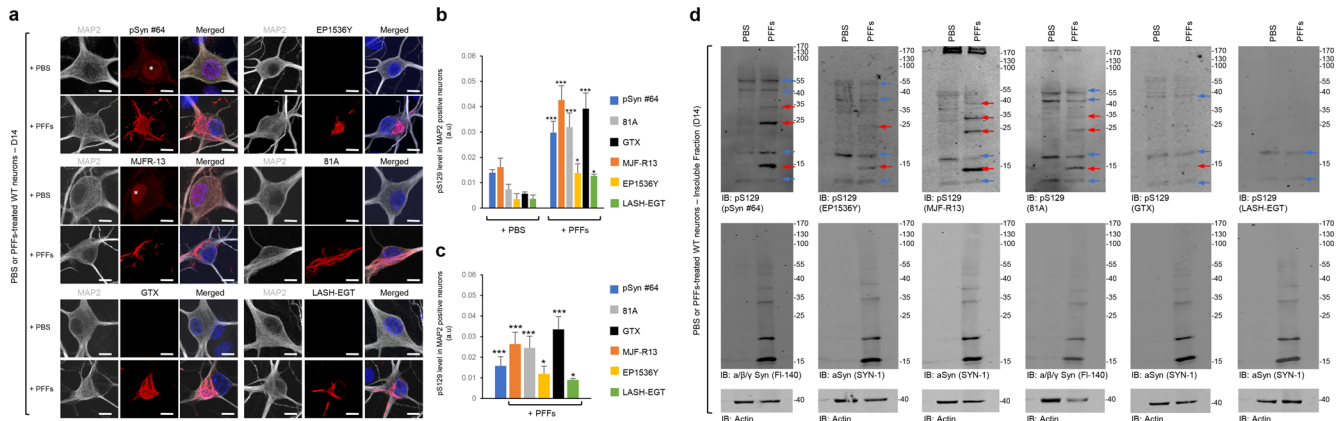
Fig. 4 Assessment of pS129 antibodies detection in the PFFs-seeded WT primary hippocampal neurons. After 14 days of treatment with 70 nM of mouse aSyn PFFs or PBS buffer (negative control), primary hippocampal neurons were fixed or lysed, and ICC (**a–c**) or WB (**d**) analyses were performed using pS129 antibodies (pSyn#64, MJF-R13, 81A, EP1536Y, and GTX or LASH-EGT). **a–c** Newly formed fibrils were detected by confocal imaging (**a**) and quantified by a high-throughput wide-field cell imaging system as previously described[35]. **b, c** Neurons were counterstained with MAP2 antibody and the nucleus with DAPI staining. Scale bar = 10 μM. **b** The left-hand side part of the histogram shows the background of each pS129 antibody in PBS-treated primary neurons, while the right-hand side part of the histogram shows the pS129 level detected by the pS129 antibodies in PFFs-treated primary neurons. **c** pS129 level in PFF-treated primary neurons was re-evaluated after subtracting the pS129 background level from the PBS-treated neurons. The graphs represent the mean +/− SD of three independent experiments. *$p < 0.01$, ***$p < 0.0001$ (ANOVA followed by Tukey HSD post hoc test, PBS vs. PFF-treated neurons). **d** WB analyses of the insoluble fractions of the PBS- and PFF-treated neurons. Membranes were then counterstained by total aSyn antibodies (SYN-1 or Fl-140 α/β/γ synuclein), and actin was used as a loading control. The red arrows indicate the pS129-aSyn positive bands. The blue arrows indicate the undefined bands. All blots were derived from the same experiment and were processed in parallel.

neighboring phosphorylation or truncation events (e.g., 81A) are sensitive to other modifications (e.g., nitration). These observations underscore the importance of always using multiple pS129 antibodies with well-characterized specificity towards the diversity of modified forms of the protein.

C-terminal truncations affect the detection of aSyn pS129 level in primary neurons

Next, we screened the ability of the antibodies to detect pS129-aSyn aggregates in a neuronal seeding model[34,35] where newly formed aggregates were shown to exhibit a PTM profile[32] resembling that of LBs in human brains[1]. Namely, phosphorylation at S129, C-terminal cleavage at multiple sites (103, 114, 119, 121, 129 and 135), and ubiquitination at multiple lysine residues[32] (Fig. 1b). We compared the ability of the six antibodies (Fig. 1c) to detect pS129 in neurons treated with aSyn PFFs[35]. After 10 days of treatment, neurons were fixed, and ICC was performed. Confocal imaging showed that the six antibodies detected S129 phosphorylated aSyn inside the seeded-aggregates in MAP2 positive neurons (Fig. 4a). Quantification of images acquired by a high-throughput wide-field cell imaging system (HTS) robustly demonstrated that the pSyn#64, 81A, MJF-R13, and GTX antibodies were the most efficient in detecting pS129-aSyn seeded-aggregates (Figs. 4b, c and S6A). These findings suggest that the pS129 antibodies differentially detect aSyn fibrillar aggregates in neurons. Two of the four antibodies, pSyn#64 and MJFR-13, showed nuclear background signal in PBS-treated neurons (Fig. 4a, white stars).

Next, we compared the specificity of the six antibodies towards aSyn aggregates isolated from the neuronal seeding model by WB analysis (Figs. 4d and S6B). The GTX and LASH-EGT antibodies did not show any pS129 signal. The pSyn#64, EP1536Y, MJF-R13, and 81A antibodies detected several undefined bands in the control samples from neurons treated with PBS. Two undefined bands occur just above and below where aSyn typically runs, as evidenced by comparing the samples from PBS and PFF-treated neurons (Fig. 4d). Furthermore, these antibodies also detect higher molecular weight bands between 35–55 kDa (pSyn#64, EP1536Y, MJF-R13, and 81A) and above 170 kDa (MJF-R13 and 81A). In the

case of the samples from PFF-treated neurons, all four antibodies detect the 15 kDa band and the undefined 17 kDa and additional higher bands that appear to be aSyn specific as they were not detected in the samples from PBS neurons (Fig. 4d).

Our findings underscore the importance of including the appropriate control samples to ensure accurate assignment of the aSyn bands by WBs. The aSyn bands between 25 and 40 KDa are frequently referred to as HMW or oligomeric aSyn species. However, previous studies from our laboratory[32] and others[1,2,36] suggest that they represent ubiquitinated forms of aSyn, which are breakdown products from HMW aggregates, including fibrils.

Not all the pS129 antibodies can capture the morphological diversity of the pS129-aSyn seeded-aggregates

We have recently shown that the nature of the PFF seeds is a strong determinant of the morphological diversity of aSyn aggregates we detect in our seeding neuronal model of LB-like inclusion formation. When hippocampal or cortical primary neurons are treated with mouse WT PFF, newly formed fibrils appear mainly as filamentous- and ribbon-like aggregates or LB-like inclusions at D21[35,37] (Supplementary Fig. 7A). In contrast, when hippocampal or cortical primary neurons are treated with PFFs derived from the newly identified human aSyn mutant E83Q, we observe a greater morphological diversity, as evident by the detection of up to six distinct morphologies, namely, the nuclear (Supplementary Fig. 7B)-, the granular-, the filamentous and granular-, the filamentous- and the filamentous-like seeded aggregates as well as the dense- and the ring-like LBs[37] (Fig. 6). Therefore, we used this model to evaluate the ability of the top four pS129 antibodies (MJF-R13, GTX, 81A, or pSyn#64) to capture the morphological diversity of aSyn pathology in primary neurons. The LASH-EGT and the EP1536Y antibodies were excluded from the screen for the following reasons: (1) the LASH-EGT antibody due to its poor capacity to recognize aSyn pathology in PFF-treated neurons (Fig. 4b, c); and (2) because the new EP1536Y antibody batches we recently acquired were no longer suitable for ICC, as acknowledged by Abcam by removing the ICC recommendation from their datasheet (https://www.abcam.com/alpha-synuclein-phospho-s129-antibody-ep1536y-ab51253.html).
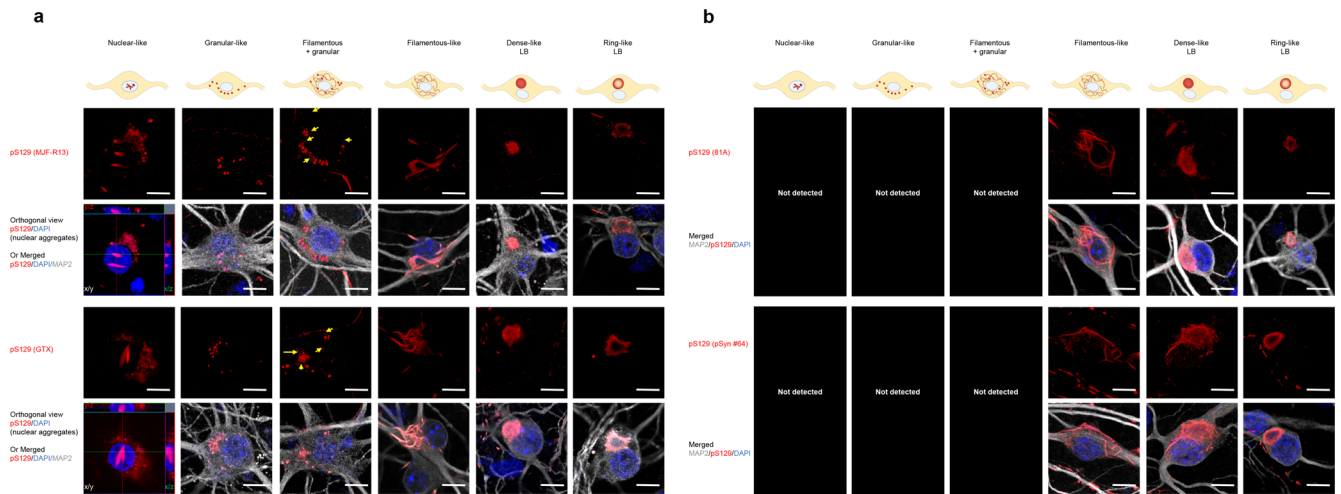
Fig. 5 All the pS129 antibodies do not detect the morphological diversity of the pS129-aSyn seeded-aggregates formed in human PFF-treated cortical neurons. a, b After 21 days of treatment with 70 nM of human E83Q aSyn PFFs, primary cortical neurons were fixed, and ICC was performed. The seeded-aggregates were detected using the pS129 antibodies (MJF-R13, GTX, 81A, or pSyn#64). Neurons were counterstained with the MAP2 antibody and the nucleus with DAPI staining. Scale bar = 10 µM. All four pS129 antibodies were able to distinguish the seeded-aggregates with the filamentous-like morphology and the LB-like inclusions with the dense core and the ring-like morphology. However, only the MJF-R13 and GTX antibodies were able to detect the nuclear, granular or granular and filamentous-like aggregates (**a**). The yellow arrows indicate the filamentous-like aggregates imbricated between the granular-like aggregates. The orthogonal view from different planes (x/y, x/z, and y/z) of the "nuclear-like" pS129-aSyn aggregates stained with MJF-R13 or GTX antibodies as well as the Imaris 3D animations (see Videos in SI files) confirmed their intranuclear localization. The schematic representation of the different types of seeded-aggregates was created using BioRender.com.

We chose to perform this study in primary cortical neurons as the neuropathological characterization of the human brain of the E83Q mutation carrier showed the highest pathology in the cortex[38]. Confocal imaging shows that all the four pS129 antibodies were able to detect the newly seeded-aggregates with the filamentous-like morphology, the LB-like inclusions with the dense core resembling cortical LBs[17,39–44] or LB-like inclusions with a ring-like morphology resembling brainstem/nigral LBs[17,19,20,39,45–47], at D21 in both human E83Q and mouse WT PFF-treated cortical neurons (Figs. 5 and S7). However, only the MJF-R13 and GTX antibodies could also detect the presence of the nuclear, granular, or granular and filamentous-like aggregates formed at D21 in the E83Q PFF-treated cortical neurons (Fig. 5). These results are not consistent with a previous report by Grassi et al.[48,49], suggesting that the GTX antibody detects only dot-like/granular structures.

Overall, in our hands, the MJF-R13 antibody is one of the best pS129 antibodies that allows thoroughly analyzing aSyn pathology formed in the primary neuronal seeding model. This antibody not only allows characterizing aSyn pathology at the biochemical level by disclosing the specific HMWs related to the seeded aggregates (Fig. 4) but also it is the best for capturing the morphological diversity of the seeded aggregates formed in neurons by ICC (Fig. 5).

Taken together, these results demonstrate that not all commercially available pS129 antibodies can capture the diversity of aSyn aggregates in the neuronal seeding model to the same extent. This highlights the importance of using multiple antibodies to characterize cellular models of aSyn pathology and identify which antibody or combination of antibodies is the most appropriate for capturing the diversity of aggregates or specific aggregate morphology of interest.

Specificity and cross-reactivity of the pS129 antibodies in primary neurons

Consistent with a previous study[11], ICC combined with confocal imaging revealed that some of the pS129 antibodies showed unspecific immunoreactivity in the cytosol or the nucleus of primary neurons. This prompted us to assess further the specificity of the six antibodies for ICC and WB analyses in neurons lacking aSyn (KO neurons) and treated with PFFs. Under these conditions, the internalized PFFs undergo rapid cleavage at residue 114, thus eliminating the epitopes for all the pS129 antibodies. Several pS129 antibodies exhibited non-specific labeling in aSyn KO hippocampal and cortical primary neurons by ICC. For example, confocal imaging revealed that the pSyn#64 and MJF-R13 antibodies detect an unspecific and intense signal in the cytosol of the hippocampal (Supplementary Fig. 8A) and cortical (Supplementary Fig. 8B) primary neurons despite a very low laser intensity (~1–2.5%) and using a photomultiplier (PMT) gain of around 600. On the other hand, the 81A and the LASH-EGT antibodies showed a similar background but only at a much higher laser intensity (~8%) (Supplementary Fig. 8). Under these conditions, we also observed that the pSyn#64, MJF-R13, and the LASH-EGT antibodies had a strong reactivity in the nucleus of both the hippocampal and cortical KO (Supplementary Fig. 8) but also WT (Fig. 4a) neurons. These findings are consistent with previous reports demonstrating that MJF-R13, pSyn#64, and 81A antibodies show extensive staining and cross-reactivity in aSyn KO mice neuronal cultures[11].

Conversely, no non-specific and/or background signal was observed in primary neurons stained with the GTX or the EP1536Y antibody, even with ~8% laser intensity (Supplementary Fig. 8). Using neurons containing pS129 positive aggregates (Fig. 4a and Supplementary Fig. 9), we found that adjusting the setup of the laser intensity and the PMT gain and offset helped eliminate the unspecific signal initially observed in the untreated or PFF-treated aSyn KO primary neurons (Supplementary Figs. 8C, D and 9).

Altogether, these results underscore the critical importance of using the appropriate positive (recombinant pS129 or neurons containing pS129 positive aggregates) and negative (aSyn KO cells/tissues) controls to allow for identifying off-target proteins and signals recognized by pS129 antibodies.
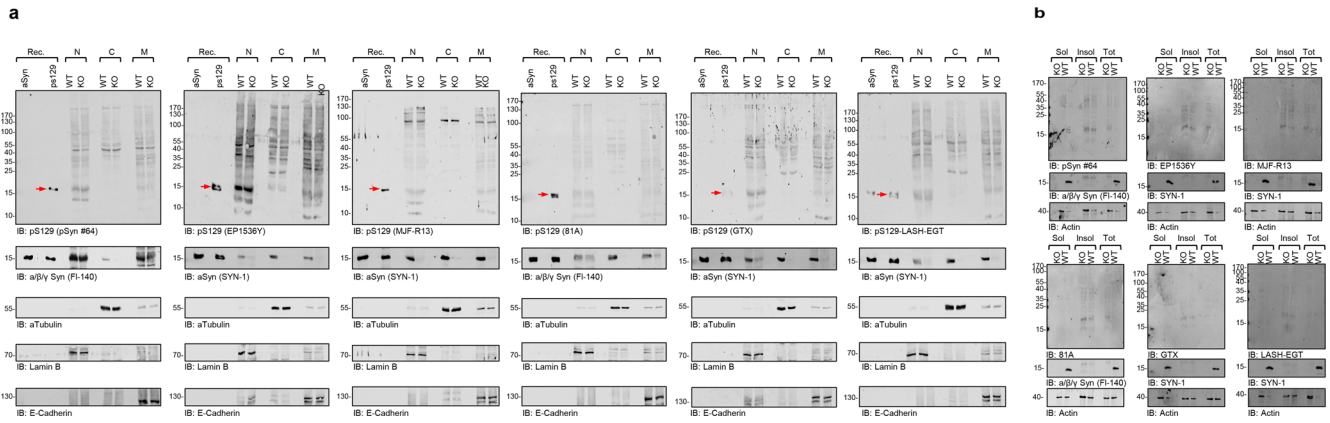
Fig. 6 Assessment of pS129 antibodies detection in the nuclear, cytosolic, and membranous fractions of aSyn KO and WT primary hippocampal neurons by WB. a, b Sequential biochemical extraction was performed on aSyn KO and WT primary hippocampal neurons cultured for 14 days (DIV14), and the pS129 level was assessed in the nuclear (N), cytosolic (C), and membrane (M) fractions (**a**) or in the soluble (sol) and insoluble (insol) fractions (**b**) by WB using the six pS129 antibodies (pSyn#64, MJF-R13, 81A, EP1536Y, GTX, and LASH-EGT). Forty nanograms of recombinant aSyn WT or phosphorylated at residue S129 (pS129, indicated by the red arrow) were used as positive controls. The pS129 antibodies were used at a dilution of 1/1000. Membranes were then counterstained by total aSyn antibodies (SYN-1 or Fl-140 α/β/γ synuclein). aTubulin, Laminin B, and E-Cadherin were used as loading control for the cytosolic, nuclear, and membrane fractions, respectively (**a**). Actin was used as a loading control for the soluble and insoluble fractions (**b**). All blots were derived from the same experiment and were processed in parallel.

All pS129 antibodies cross-react with several nuclear proteins that could be mistaken for full-length, truncated, and oligomeric forms aSyn

Initial studies reported increased accumulation of pS129 with age in the cortical brain areas and dopaminergic neurons of aSyn transgenic mice[50,51]. In these studies, pre-treatment with phosphatases resulted in the disappearance of the pS129 immunoreactivity. Wakamatsu et al. also reported that nuclear aSyn is preferentially phosphorylated compared to cytosolic aSyn[51]. However, most of these studies were based on IHC/ICC and relied on the use of a single pS129 antibody[51–55] (Supplementary Fig. 1). Furthermore, the cross-reactivity of pS129 antibodies towards nuclear proteins has not been systematically assessed. We previously reported that some PD-linked mutations, such as E46K, enhance aSyn nuclear localization and detection of pS129 by ICC but failed to detect an increase in pS129-aSyn by WB[56]. We speculated that this could be due to the presence of predominantly truncated and phosphorylated C-terminal fragments of aSyn in the nucleus. To help address such discrepancies and identify better tools for assessing nuclear pS129-aSyn, we evaluated the specificity of the six pS129 antibodies towards nuclear (N), cytosolic (C), and membrane-associated proteins (M) but also the soluble and insoluble fractions by performing biochemical subcellular fractionation of lysates from neurons (Fig. 6) and mammalian cells (Supplementary Figs. 10 and 12).

First, we assessed by WB the pS129 levels in the nuclear, cytosolic, and membrane fractions (Fig. 6a) and the soluble/insoluble fraction (Fig. 6b) of the primary hippocampal neurons from WT and aSyn KO mice. We observed a strong cross-reactivity with several proteins of various sizes, particularly in the nuclear and membrane fractions (Fig. 6a), where all pS129 antibodies show prominent detection of a 16–17 kDa band that exhibits similar SDS-PAGE mobility to that of full-length aSyn and truncated recombinant aSyn species usually detected in neuronal aSyn seeding models. These bands were observed in the nuclear fractions from WT and KO neurons, thus establishing that they do not represent aSyn species. Interestingly these bands were absent in the cytosolic fractions. However, all pS129 antibodies also showed cross-reactivity to several proteins with molecular weight ranging from 25 to ~200 kDa (Fig. 6).

As mammalian cell lines are frequently used to study the cell biology of aSyn, investigate its aggregation mechanisms, and

screen for modifiers of aSyn aggregation, we also evaluated the specificity of the pS129 antibodies towards soluble and insoluble proteins from HEK and HeLa cells transfected with WT aSyn plasmid or empty vectors. All six antibodies showed undefined detection of several bands in both cell lines, with the 17 KDa species being the most abundant, mainly in the insoluble fractions (Supplementary Fig. 10). There was no difference in the bands detected in cells transfected with aSyn plasmids or an empty vector. Although the intensity of the 17 kDa band increased in cells overexpressing aSyn, monitoring aSyn levels using a pan-aSyn antibody suggests that it is unlikely that this band corresponds to phosphorylated aSyn proteins. Interestingly, more undefined bands were detected in the soluble and insoluble fractions from HEK cells. Furthermore, EP1536Y detected more undefined bands in the soluble fractions than the other five antibodies.

Interestingly, the same prominent nuclear bands pattern observed in primary neurons was also detected in the nuclear fractions from mammalian cells (HeLa and HEK293) transfected with WT aSyn or an empty vector (Supplementary Fig. 11). Notably, the pattern of proteins that cross-react with pS129 in the membrane fractions was distinct from that seen in the nuclear fractions. Furthermore, the undefined bands seen in the nuclear fraction exhibit similar but not identical mobility to that of newly formed fibrils seen in many of the aSyn seeding-based neuronal models, including the appearance of two prominent bands with MW of ~16–17 and ~13–12 kDa, similar to that of full-length and truncated aSyn species, in addition to a band at ~50 kDa and other HMW species. The small differences in size in relation to WT aSyn can be discerned more easily using Tricine gels (Supplementary Fig. 12). Taken together, these findings demonstrate that all pS129 antibodies show strong cross-reactivity with membrane and nuclear proteins. The pattern of pS129 non-specific immunoreactivity detected by WB could be mistaken for pS129 species seen in the aSyn neuronal seeding models. It is noteworthy that under conditions where significant pS129 immunoreactive aSyn aggregates are formed, these non-specific bands become less prominent[37]. These findings underscore the importance of not only validating the pS129 antibodies but also using the appropriate (1) control samples (e.g., recombinant WT and pS129 and lysates from aSyn KO neurons or cells that do not
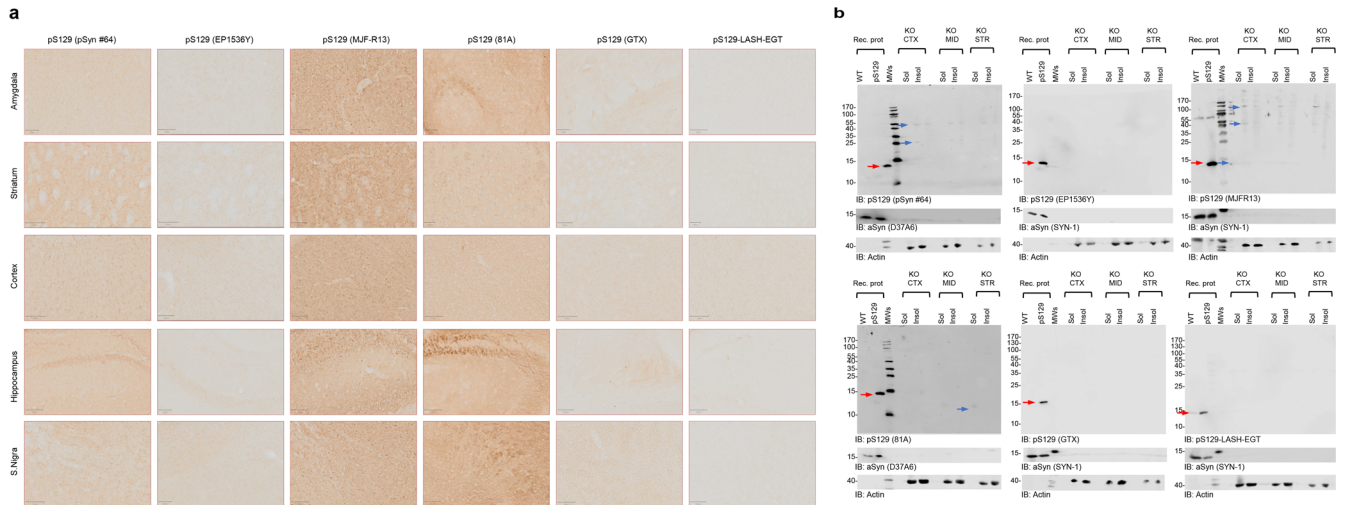
Fig. 7 Assessment of pS129 antibodies detection in brain sections of aSyn KO mice. a Brain coronal sections (50 μM thick) from different brain areas of aSyn KO mice (Amygdala, Striatum, Motor Cortex, Hippocampus and Substantia Nigra) have been examined to assess the different staining patterns of the six pS129 antibodies (pSyn#64, MJF-R13, 81A, EP1536Y, GTX, and LASH-EGT). Scale bar = 100 μM. **b** pS129 level of detection in the soluble and insoluble fractions extracted from the aSyn KO mice brains using the six pS129 antibodies (pSyn#64, MJF-R13, 81a, EP1536Y, GTX, and LASH-EGT). Sequential biochemical extraction was performed on different brain regions (cortical/CTX; Midbrain/MID and Striatum/STR) derived from aSyn KO mice, and the level of pS129 was assessed in the soluble (0.1% Triton-soluble fraction) and the insoluble fraction (2% SDS-soluble fraction). 40 ng of recombinant aSyn WT or phosphorylated at residue S129 (pS129, indicated by the red arrow) were used as positive controls. Membranes were counterstained for total aSyn (SYN-1 or D37A6), and actin was used as a loading control. The red arrows indicate the pS129-aSyn-positive bands. The blue arrows indicate the undefined bands. All blots were derived from the same experiment and were processed in parallel.

express aSyn); and (2) SDS-PAGE gels that allow clear separation of proteins between 10-20 KDa (e.g., Tricine gels).

Some pS129 antibodies display unspecific signals in aSyn KO mouse tissue

To further assess the specificity of the pS129 antibodies in brain tissues, we stained tissue from different brain regions, including the amygdala, striatum, cortex, hippocampus, and substantia nigra, from aSyn KO animals (Fig. 7a). The EP1536Y, GTX, and LASH-EGT antibodies did not show any background staining in all five regions. The MJF-R13 and 81A antibodies showed high background in all five regions, especially in the hippocampus, substantia nigra (81A), amygdala and striatum (MJF-R13). The MJF-R13 staining showed mostly dotted structures around the nuclei or staining the nucleus itself, whereas the 81A showed mostly neuritic staining, especially in the hippocampus and substantia nigra. The pSyn#64 antibody showed an intermediate background with the highest background signal seen in the striatum and hippocampus. The high background signal of the 81A and pSyn#64 antibodies could be because these two antibodies are raised in the same species (mouse) of the target tissue (mouse). On the other hand, this does not explain the strong neuritic staining present in the hippocampus of 81A-stained tissue (Fig. 7a). In our hands, the LASH-EGT and GTX antibodies are highly specific to pS129 and do not recognize other proteins when used for IHC application. Our results are in line with a previous report by Delic et al. where MJF-R13 exhibited the highest background revealed as punctate intracellular structures and the 81A antibody displayed an off-target signal reminiscent of neuronal processes[4].

Furthermore, Delic et al. also reported that EP1536Y shows the highest specificity with little to no off-target labeling and the same order of background signal as shown in Fig. 7a[4]. In a recent study, Arlinghaus et al. showed that three pS129 antibodies (MJF-R13, pSyn#64, and EP1536Y) showed cross-reactivity in brain slices and primary cultures (by IHC or ICC)[11]. Similar to what we report, Arlinghaus and colleagues show that MJF-R13 and pSyn#64 stained cell bodies throughout all regions analyzed, with

no differences between WT and *SNCA* KO mouse tissues[11]. 81A did not show cell body staining but displayed higher background in the cortex and substantia nigra than in other areas. We also highlighted that 81A did not show somatic staining but rather a neuritic off-target signal. Nevertheless, we detected higher background in the substantia nigra, amygdala, and especially the hippocampus, with little to no background in the cortex. In contrast to our findings, they also report that EP1536Y displays somatic staining, whereas we detected little to no unspecific signal.

To better understand the sources of the background signals, we assessed the specificity of the antibodies in the cortex, midbrain, and striatal lysates from aSyn KO animals (Fig. 7b). The three antibodies (EP1536Y, GTX, and LASH-EGT) that did not show a background signal by IHC also did not show any bands by WB. Even at high exposure, we only observed one HMW band at ~120 kDa for the LASH-EGT antibody (Supplementary Fig. 13). In contrast, the MJF-R13 showed several bands ranging from 25 to 170 kDa in the soluble and insoluble fractions of lysates from the three brain regions, consistent with the high background signal observed by IHC (Fig. 7a). The pSyn#64 antibody, at high exposure, showed a strong signal for a band with a molecular weight that runs slightly higher than aSyn and HMW bands. The 81A shows a single band with a molecular weight below 15 kDa in the soluble fractions from the midbrain and striatal tissue lysates (Fig. 7b). These results are in line with those described by Delic and colleagues, which also revealed the highest off-target signal for MJF-R13[4].

Nevertheless, in our hands, the EP1536Y antibody did not present any undefined high molecular weight bands, probably due to differences in the composition of the extraction buffers used in the two studies. Similarly, Delic et al. report that the 81A antibody shows a single 75 kDa band when using SDS extraction buffer[4], whereas in our case, a lower band appears at higher exposure in the Triton-soluble fraction, but not in the insoluble fraction (Supplementary Fig. 13). Overall, these findings are consistent between WB and IHC and demonstrate that some of the commonly used antibodies (e.g., 81 A and MJF-R13) are not
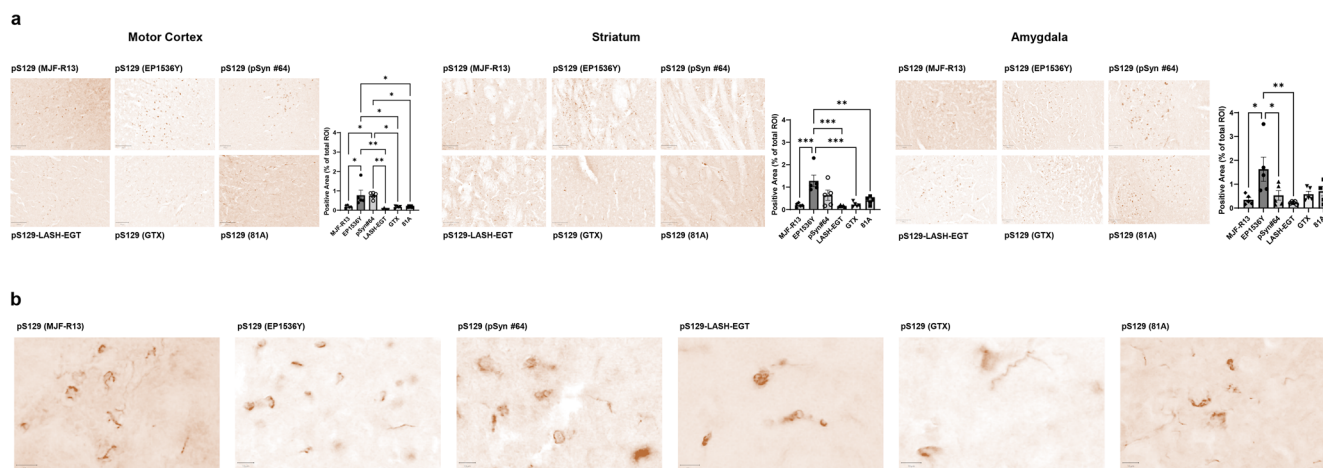
Fig. 8 Evaluation of staining pattern of aSyn pathological aggregates in WT PFF-injected mice. a Brain coronal sections (50 μM thick) from different brain areas of C57BL6/J PFF-injected mice (Amygdala, Striatum, Motor Cortex), 3 months post-injection, have been examined to assess the different staining patterns of the six pS129 antibodies (pSyn#64, MJF-R13, 81A, EP1536Y, GTX, and LASH-EGT). Scale bar = 100 μM. Quantification for each area has been carried out using Qupath and was expressed as a percentage of positive area stained of total ROI. Data are presented as means ± SEM. *$p < 0.05$, **$p < 0.01$, ***$p < 0.001$ according to one-way ANOVA followed by the Tukey test for multiple comparisons. **b** Microphotographs of the amygdala were stained with the six pS129 antibodies (pSyn#64, MJF-R13, 81A, EP1536Y, GTX and LASH-EGT) at higher magnification. Scale bar = 10 μM.

specific to aSyn and recognize other proteins in the brain. Among all the antibodies tested, EP1536Y and GTX appear to be the most specific for pS129.

pS129 antibodies display different staining patterns in aSyn mPFF-injected WT mice based on the brain region analyzed

To determine if the pS129 antibodies exhibit differential immunoreactivity towards different aSyn pathological aggregates, we stained brain slices from WT mPFF-injected mice 3 months after injection (Fig. 8). In the motor cortex, all six antibodies were able to capture, to a different extent, neuritic and somatic aSyn aggregates (Fig. 8). Nevertheless, EP1536Y showed the strongest staining of aSyn aggregates, with similar immunoreactivity towards neuritic or somatic aggregates. The appearance of these aggregates varies from skein-like structures to long serpentine neuritic and dense perinuclear aggregates. In contrast, MJF-R13 and pSyn#64 showed weaker staining, with a slight preference of MJF-R13 towards perinuclear aggregates and some partial fibrillary neuritic staining, whereas 81A greatly privileged fibrillary neuritic staining (Fig. 8).

In the striatum, pSyn#64 consistently showed a preference for detecting dense perinuclear aggregates and skein-like aggregates, although once again underestimating a load of aSyn pathology, compared to EP1536Y, MJF-R13 and LASH-EGT, in this brain region, highlighted mild aSyn pathology without any preference for neuritic vs. somatic pathology and revealed diffuse cytoplasmic aggregates, as well as skein-like and neuritic tubular structures. On the other hand, GTX and pSyn#64 underperformed in terms of pathological load evaluation compared to EP1536Y, which, once again, proved to be the antibody that most reliably detects pathological aggregates, including the dense round cytoplasmic aggregates. Finally, in the amygdala, all antibodies were able to equally reveal the high level of pathological load, except for MJF-R13, which only partially stained pS129-positive inclusions. Interestingly, in this region, the pSyn#64 antibody displayed better the diversity of the aggregates (Fig. 8). It is also interesting to note that EP1536Y displayed a preference toward dense intracytoplasmic inclusions over aggregates in neuronal processes, which appeared more prominent with the other antibodies. The GTX antibody showed highly variable staining patterns from animal to animal. Consistent with a previous study by Delic and colleagues, EP1536Y showed the highest signal

specificity and captured better the different forms of aSyn aggregates. Nevertheless, in our hands, MJF-R13 did not reveal as much pathology load as reported by Delic and colleagues in the striatum. Under our experimental conditions, all the antibodies displayed a similar capacity to stain aSyn aggregates with a similar propensity towards long neuritic aggregates (Fig. 8). In addition, we have also assessed the ability of the pS129 antibodies to detect the neuritic vs. cell body pathology or the morphological differences (skin-like inclusions vs. dense inclusions) of the seeded aggregates. Again, the EP1536Y antibody gave the best results in terms of capturing the morphological diversity of aggregates and their presence in different subcellular localization (neuritic and cell body aSyn aggregates) in all regions examined. In the striatum, the pSyn#64 also performed noticeably well, while detection of aSyn aggregates by 81A was limited mainly to the neurites (skin-like or dense aggregates). Similarly, MJF-R13 robustly detected pathology but staining of neuritic aggregates was less prominent. In the Motor Cortex, pSyn#64 performance was similar to EP1536Y, but it stained less prominently the neurites. Finally, in the amygdala, all antibodies detected the aSyn pathology load equally (except for EP1536Y). Overall, EP1536Y proved to be the most reliable antibody to assess aSyn pathology in all brain regions in mouse tissue. The differential sensitivity and specificity of the antibodies in different brain regions could partially explain the experimental variability observed across different laboratories. Therefore, we recommend that the performance of new antibodies should be systematically assessed in different brain regions before they are used to assess and quantify aSyn pathology formation and spreading.

Identification of putative candidate proteins that cross-react with pS129

Although several studies have shown that pS129 cross-reacts with selected proteins, a systematic analysis and cataloging of all possible proteins that could cross-react with pS129 antibodies has not been performed. Therefore, we screened all known human and mouse phosphorylation sites annotated in Uniprot (https://www.uniprot.org) for sequence similarities to peptide sequences comprising not only S129 but all the other phosphorylation sites that have been detected in LBs and PD brains (Y39, S87, and Y125). In addition, we included peptide sequences comprising Y133 and Y136. Entries for humans ($n = 7662$) and mice ($n = 7133$)
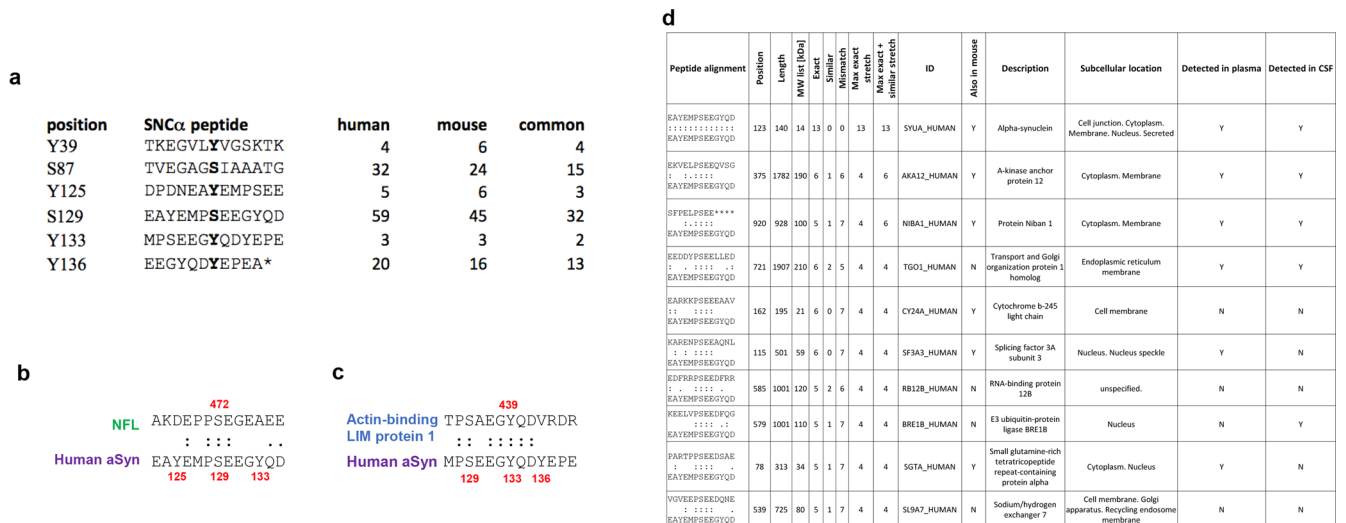
a

position	SNCα peptide	human	mouse	common
Y39	TKEGVL**Y**VGSKTK	4	6	4
S87	TVEGAG**S**IAAATG	32	24	15
Y125	DPDNEA**Y**EMPSEE	5	6	3
S129	EAYEMP**S**EEGYQD	59	45	32
Y133	MPSEEG**Y**QDYEPE	3	3	2
Y136	EEGYQD**Y**EPEA*	20	16	13

b

```
                472
NFL        AKDEPPSEGEAEE
           :  :::     ..
Human aSyn EAYEMPSEEGYQD
           125   129   133
```

c

```
                          439
Actin-binding  TPSAEGYQDVRDR
LIM protein 1     ::  :::::
Human aSyn     MPSEEGYQDYEPE
               129    133  136
```

d

Peptide alignment	Position	Length	MW list [kDa]	Exact	Similar	Mismatch	Max exact stretch	Max exact + similar stretch	ID	Also in mouse	Description	Subcellular location	Detected in plasma	Detected in CSF
EAYEMPSEEGYQD ::::::::::::: EAYEMPSEEGYQD	123	140	14	13	0	0	13	13	SYUA_HUMAN	Y	Alpha-synuclein	Cell junction. Cytoplasm. Membrane. Nucleus. Secreted	Y	Y
EKVELPSEEQVSG : :..::: EAYEMPSEEGYQD	375	1782	190	6	1	6	4	6	AKA12_HUMAN	Y	A-kinase anchor protein 12	Cytoplasm. Membrane	Y	Y
SFPELPSEE**** .:..::: EAYEMPSEEGYQD	920	928	100	5	1	7	4	6	NIBA1_HUMAN	Y	Protein Niban 1	Cytoplasm. Membrane	Y	Y
EEDDYPSEELLED . .::: .: EAYEMPSEEGYQD	721	1907	210	6	2	5	4	4	TGO1_HUMAN	N	Transport and Golgi organization protein 1 homolog	Endoplasmic reticulum membrane	Y	Y
EARKKPSEEEAAV :: .:::: EAYEMPSEEGYQD	162	195	21	6	0	7	4	4	CY24A_HUMAN	Y	Cytochrome b-245 light chain	Cell membrane	N	N
KARENPSEEAQNL : .:::: EAYEMPSEEGYQD	115	501	59	6	0	7	4	4	SF3A3_HUMAN	Y	Splicing factor 3A subunit 3	Nucleus. Nucleus speckle	Y	N
EDFRRPSEEDFRR : . .::: . EAYEMPSEEGYQD	585	1001	120	5	2	6	4	4	RB12B_HUMAN	N	RNA-binding protein 12B	unspecified.	N	N
KEELVPSEEDFQG .:..::: . EAYEMPSEEGYQD	579	1001	110	5	1	7	4	4	BRE1B_HUMAN	N	E3 ubiquitin-protein ligase BRE1B	Nucleus	N	Y
PARTPPSEEDSAE : .:::: EAYEMPSEEGYQD	78	313	34	5	1	7	4	4	SGTA_HUMAN	Y	Small glutamine-rich tetratricopeptide repeat-containing protein alpha	Cytoplasm. Nucleus	Y	N
VGVEEPSEEDQNE . :::: . EAYEMPSEEGYQD	539	725	80	5	1	7	4	4	SL9A7_HUMAN	N	Sodium/hydrogen exchanger 7	Cell membrane. Golgi apparatus. Recycling endosome membrane	N	N

Fig. 9 Identification of putative candidate proteins that could cross-react with aSyn antibodies. a List of peptides used to search the Uniprot database to identify putative proteins that could cross-react against antibodies raised against the known aSyn phosphorylated residues highlighted in bold at the middle of each sequence. The number of candidate hits retrieved for human, mouse, or common to both organisms is indicated for each peptide. The asterisk (*) present in the last sequence indicates the C-terminal residue. **b** Sequence alignment of the region around human aSyn pS129 and Neurofilament light polypeptide (NFL) pS472, which is known to cross-react with antibodies raised against pS129-aSyn. **c** Sequence alignment of the region around human aSyn pY133 and Actin-binding LIM protein 1 pY439, illustrating the high level of similarity. **d** List of the top ten candidate proteins that can cross-react with pS129 antibody.

were retrieved as full text. A Perl script was then used to parse the entries and extract protein sequence fragments of 13 residues centered on the annotated phosphorylation sites to compare them to the six human aSyn fragments. Figure 9a shows the hits of only those whose residues preceding and following the phosphorylation site were perfect matches. For all protein fragments retrieved from Uniprot satisfying this condition (Supplementary Fig. 14), we computed the number of exact and highly similar matches to the six aSyn fragments shown in Fig. 9a and the length of the continuous stretch of perfect or similar matches encompassing the phosphorylation site (see material and method section for details).

The highest number of hits was returned with the search using the S129 anchor peptide, with 59 and 45 human and mouse hits, respectively, of which 32 are in common (Fig. 9a and Supplementary Fig. 14). This is, for example, the case for the NFL, which has been reported to cross-react with antibodies raised against fragments of aSyn pS129[9]. Interestingly, NFL was ranked 44 (out of 59) and 35 (out of 45) for human and mouse, respectively (Supplementary Figs. 14 and 15). Furthermore, it bears a modest local similarity with the aSyn fragment, where both protein fragments share a continuous stretch of three conserved residues, a fourth disjoint but conserved residue and two further residues with high similarity scores (Fig. 9b). This indicates that several other hits have sequences that are locally even more similar to the aSyn S129 fragment than NFL, several bearing continuous stretches of four fully conserved residues as well as additional similar residues and may consequently also cross-react with pS129 antibodies, depending on their local structure and experimental conditions. Based on the local conservation metric, the best candidate for cross-reaction is the Actin-binding LIM protein 1, which shares a local stretch of five conserved residues with the phosphorylated Y133 aSyn region along with two additional fully conserved residues nearby Fig. 9c.

Of note, the list of candidate proteins that could cross-react with antibodies raised against phosphorylated aSyn is likely not exhaustive because the hits reported are limited to phosphorylation sites annotated in Uniprot at the time of the search (Fig. 9d and tables in Supplementary Fig. 14). For example, among the six aSyn seed fragments used to scan the database, only three

identify aSyn as a candidate protein (S87, Y125, and S129). These three residues are currently annotated as phosphorylated in Uniprot (https://www.uniprot.org). Only Y125 and S129 return aSyn as a hit for mice because an asparagine that cannot be phosphorylated is present at position 87 instead of a serine. The fact that a hit is found both in humans and in mice does not per se reflect a higher potential for cross reactivity. Instead, this merely reflects that a phosphorylation site is not necessarily conserved between human and mouse proteins, as mentioned above for aSyn at position 87, or that the two residues surrounding the phosphorylation site are not strictly conserved between human and mouse, a condition imposed during our scanning strategy. Nevertheless, taken collectively, these hits represent a list of candidate proteins that should be considered for putative cross reaction with antibodies raised against phosphorylated aSyn fragments.

As a next step, we investigated how many of these candidate proteins that could cross-react with pS129 antibodies were previously identified in biological specimens. From the total number of candidate proteins based on the peptide alignment ($n = 123$) that could potentially cross-react with the different aSyn PTMs (i.e., pS129, pS87, pY39, pY125, pY1233, and pY136) (Supplementary Fig. 14), 47.97% ($n = 59$) and 32.52% ($n = 40$) were previously reported to be detected in human plasma and cerebrospinal fluid (CSF), respectively. Particularly, when focusing on the proteins ($n = 59$) that could react with pS129, the percentage of proteins previously identified in plasma was 45.8% ($n = 27$) and 32.2% ($n = 19$) in CSF. Several other proteins were also identified to potentially cross react with the other aSyn PTMs, in plasma and CSF (Supplementary Fig. 14A).

Whether cross-reactivity with some of these candidate proteins could be contributing to the high variability of pS129 across the different biomarker-based studies remains unknown. This is in part because the levels of the phosphorylated forms of these proteins in biological fluids are unknown. However, their presence and a high potential for cross-reactivity with phosphorylated aSyn antibodies underscore the importance of validating the specificity of pS129 antibodies in biological fluids. This could be done using CSF or plasma sample standards where the desired phosphorylated aSyn species have been depleted.

Although cross-reaction should be tested experimentally, we hope that the list of proteins we provide here (see tables in Supplementary Figs. 14 and 15) could help to better assess the specificity of future antibodies against disease-associated phosphorylation sites. The local alignments can also be scrutinized to check in more detail the similarity based on other criteria not considered during the ranking, such as the local charge.

DISCUSSION

Among all the research tools and reagents used by scientists daily, antibodies have the greatest influence on shaping our knowledge and current hypotheses about the pathophysiology of PD and neurodegenerative diseases. Therefore, it seems obvious that the use of poorly characterized antibodies or antibodies that show non-specific cross-reactivity could lead to misinterpretation of experimental observation and misdirection of time, investments, and resources[57,58]. The work presented here, combined previous studies from other groups[4,5,9,11,23], demonstrates that the development of antibodies that target specific post-translationally modified or aggregated forms (oligomers, fibrils, LNs, or LBs) aSyn remains challenging. Although most pS129 antibodies showed good performance in detecting aSyn aggregates in the cellular seeding models and PFF-injected mouse brain tissues containing abundant aSyn pathology, the level of cross-reactivity we detected in aSyn KO samples underscores the urgent need for better antibodies targeting pS129-aSyn and other modified forms of aSyn. This is even more critical when the antibodies are used to investigate the role of pS129 in regulating the physiological functions of aSyn. In this section, we reflect on the implications of our work for investigating the mechanisms underpinning aSyn pathology formation and their role in the pathogenesis of PD. We also discuss how we can apply the lessons learned from previous efforts to develop PTM and conformation-specific aSyn antibodies to establish more robust pipelines for the development, characterization and validation of such antibodies.

Today, the histopathological staging of LB diseases[59–61] and the assessment of pathology formation and spreading capacity in aSyn-based animal[62–65] and cellular[66–68] models of PD and related diseases rely mainly on antibodies targeting the C-terminal domain[59–61,69,70] of the protein and more recently pS129 immunoreactivity[2,71–73]. Very often, such studies rely on a single aSyn antibody and, more recently, primarily pS129 antibodies[73,74] (Supplementary Fig. 1).

It is now well established that aSyn in LBs is not only subjected to multiple PTMs, including phosphorylation, ubiquitination, truncation, and oxidative nitration[75,76], but also exists as a mixture of different species with different PTM patterns and localization within LBs. Previous studies have suggested that the majority (>90%) of aSyn in LBs is phosphorylated on S129 residue[1]. Therefore, when additional aSyn PTMs are detected in LBs, it is plausible to assume that a significant percentage of aSyn within LBs bears multiple PTMs. Our results demonstrate that the presence of other PTMs in close proximity to pS129 dramatically influences antibody-based detection of monomeric[77] and aggregated forms of pS129-aSyn in a site, PTM type, and PTM number dependent manner. These findings, combined with increasing evidence demonstrating that aSyn aggregates bear multiple modifications and are enriched in C-terminally truncated species, suggest that it is unlikely that antibodies against pS129 or any single C-terminal (a.a. 115–140) targeting antibody are capable of capturing the diversity of aSyn species or aSyn pathology in the brain. It is noteworthy that several studies have reported that aSyn astroglia pathology is not detectable using C-terminal targeting aSyn antibodies but can be revealed with antibodies targeting the NAC domain of the protein[61,78–81]. In a recent study, Henderson et al. reported that mice treated with the Glucocerebrosidase inhibitor conduritol-β-epoxide CBE develop spheroid structures

that are recognized by the 81A but not the EP1536Y pS129 antibody[82]. Although the molecular basis of this differential labeling by pS129 antibodies remains unclear, these observations underscore the importance of using multiple pS129 and aSyn antibodies to characterize aSyn species and pathology[4,9]. Although the aSyn sequence does not contain nuclear localization signals, several studies have reported nuclear localization of neuronal aSyn in human and rodent brains[50–52]. However, the role of nuclear aSyn in health and disease remains a subject of intense debate. aSyn interactions with DNA and histones, regulation of gene expression[54], and induction of transcriptional dysregulation[53,83] of cell cycle-related genes have been proposed to be fundamental mechanisms contributing to aSyn-induced toxicity in PD and other synucleinopathies. However, which forms of aSyn exist in the nucleus and the factors involved in regulating the aSyn life cycle in the nucleus or shuttling between the nucleus and cytoplasm remain unknown.

Several studies have focused on using this pS129-aSyn as a diagnostic biomarker of aSyn pathology in peripheral tissue and biological fluids. pS129-aSyn has been detected in different peripheral tissues, such as colon[84], skin[85], CSF[86] and plasma[87,88]. The enteric nervous system (ENS) has been proposed to play a pivotal role in the initiation and propagation of PD pathology and the gut-brain axis in PD and other synucleinopathies. Furthermore, the lack of antibodies that robustly and reliably detect pS129-aSyn in the ENS has hampered efforts to elucidate the role of aSyn phosphorylation in regulating aSyn biology and pathology formation in the ENS. While several studies have reported on the detection of pS129 by immunofluorescence, biochemical evidence for the accumulation of pS129 in the ENS and peripheral tissue remains sparse and lacks validation. However, very little is known about the aggregation state of pS129-aSyn in peripheral tissues or biological fluids. One study by Preterre et al. reported that several pS129 antibodies, including two of the six used in this study (EP1536Y and pSyn#64), failed to robustly detect pS129 by WB and lacked the specificity to detect pS129 in the gut[89].

Lassozé et al. evaluated the specificity and sensitivity of five commercially available pS129 antibodies (sc-135638, Invitrogen: #482700, ab59264, EP1536Y, and D1R1R) in primary cultures of ENS[26]. They reported that one of the five antibodies, D1R1R, was the most specific (no detection of undefined bands by WB) and reliable in detecting endogenous pS129 in primary rat cultures of ENS. Unfortunately, this study displays many shortcomings that make it difficult to draw any conclusions about their findings. First, none of the experiments included a proper positive control for pS129. For example, the antibodies were assessed for their ability to detect non-modified aSyn, but a positive control of recombinant site-specific pS129 was not included, although such standards are commercially available (Proteos, Inc. Cat#RP-004). Furthermore, no brain sample known to contain detectable levels of pS129-aSyn was included as controls in the WB analysis of the primary culture of ENS. Second, the specificity of the antibodies, including D1R1R, was not evaluated using primary cultures of ENS from SNCA KO mice. Third, a direct comparison of the performance of the five antibodies by immunofluorescence, under the condition of based and KCl-induced increase in pS129 levels, was not carried out or presented. In this regard, only the immunofluorescence data for D1R1R was presented. One surprising finding reported in this paper is their observation that three of the pS129 antibodies they used also recognize non-modified monomeric aSyn. This contrasts with our data (Fig. 2) and others[5], where we clearly show using modified and unmodified proteins that EP1536Y recognize, specifically pS129 but not the unmodified protein using standard protein concentrations of 40–100 ng.

Increasing evidence suggests that phosphorylation of aSyn regulates the structural properties[90], interactome, and subcellular localization of many aspects of aSyn physiological functions[8]. Therefore, there is an urgent need to develop antibodies that are
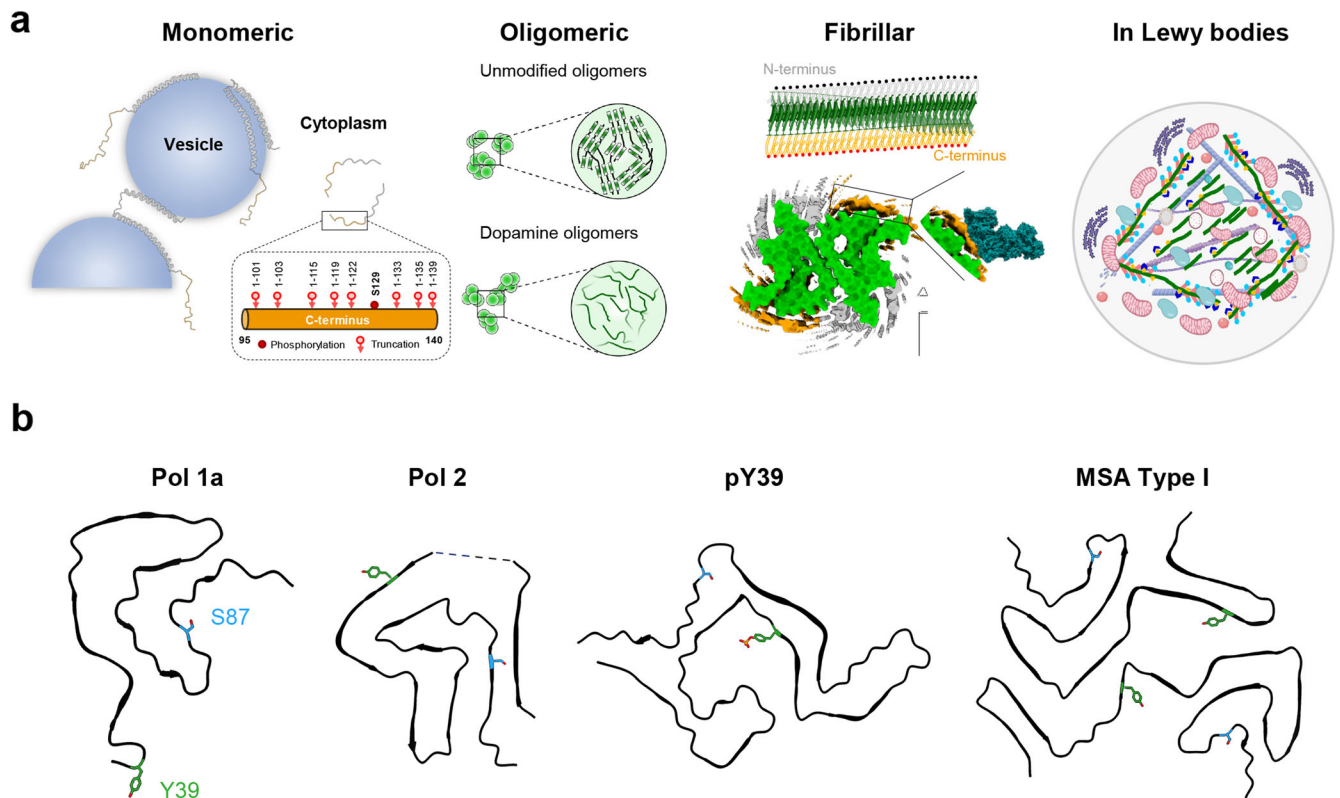
Fig. 10 The multiple faces of aSyn and their susceptibility to post-translational modifications. a The C-terminal domain of aSyn remains disordered and accessible in most aSyn species, from monomers to oligomers, fibrils, and Lewy bodies; monomeric forms of aSyn are predominantly disordered but adopt a-helical rich conformations when bound to vesicles. Despite the absence of an atomic model for aSyn oligomers, several types of aSyn oligomers of distinct conformations (disordered or b-sheet rich) and morphological properties have been observed during aSyn in vitro aggregation[91]. Near-atomic models for aSyn fibril core structures solved using cryo-EM (depicted model PDB:6CU7, EMDB: EMD-7618)[56]. On top, a schematic depiction of the fibrils showing the amyloid core sequence (green), disordered N-terminus (gray), and disordered C-terminus (orange). In all cases, the protein's C-terminus, which harbors various sites for the protein's truncation and/or phosphorylation, is disordered and accessible. aSyn fibrils found in pathological aggregates are ubiquitinated (black dots), mostly in the N-terminal domain, and phosphorylated, especially at S129 (red dots), and nitrated at multiple tyrosine residues (Y125/Y133/Y136). In LB, modified aSyn fibrils represent one of the key components of Lewy bodies and interact with a large number of proteins, membranous structure organelles, and lipids. Many of these interactions are mediated by N- and C-terminal domains that harbor several sites of PTMs. Recent studies demonstrated that these PTMs play key roles in regulating aSyn fibrils remodeling and LB formation and maturation[32,35]. **b** A selection of aSyn fibrils' cryo-EM core structures to illustrate the diversity of aSyn fibril structures and the positions of other disease-relevant PTM sites (Y39 in green and S87 in blue) present in the fibril core. One protofilament of the in vitro derived fibrils is displayed, including Polymorph 1a (Pol 1a, PDB-6CU7)[56], Polymorph 2 (Pol 2, PDB-6SST)[101] and fibrils from pY39 monomers (pY39, PDB-6L1T)[102]. An example of the fibrils derived from the postmortem brain of multiple system atrophy patients is also displayed (MSA Type I, PDB-6XYO)[103]. The LB representation in **a** was created using BioRender.com. The fibril core icon "Amyloid fibril" was adapted from BioRender.com.

capable of detecting both physiological and pathogenic pS129 species. Recently, Arlinghaus et al. described a new Proximity Ligation Assay (PLA) that allows for the specific detection of endogenous soluble pS129-aSyn in primary neurons and in mouse and human brain sections with significantly reduced background signal and cross-reactivity[11]. Their results suggest that pS129 is ubiquitously expressed throughout the mouse brain and is elevated in the cell bodies within specific brain regions, suggesting more specific roles of pS129 in these brain regions. Despite the failure of the PLA assay to detect aggregated pS129 in human brain tissues, these results are encouraging and suggest that the use of a combination of pS129 and other aSyn antibodies allows for the development of more rapid, compared to PLA, and specific assays and methods for detecting endogenous pS129-aSyn. Furthermore, Killinger et al. showed a high abundance of pS129 in the mitral cell layer of the olfactory bulb[8]. Altogether, these findings suggest a potential physiological role for S129 phosphorylation in aSyn biology and underscore the importance of developing more specific and sensitive antibodies against aSyn phosphorylated at S129 or bearing other modifications, especially given the high cross-reactivity we observed for most antibodies

under conditions of low aSyn expression or in absence of aSyn aggregates.

Increasing evidence shows that physiological and aggregated forms of aSyn exist in different conformational states and exhibit distinct interactomes (Fig. 10). Although most existing structural data suggest that the regions harboring the majority of aSyn PTMs (extreme N- and C-terminal domains) remain flexible and accessible, this by no means guarantees that antibodies targeting PTMs in these regions would be capable of capturing this diversity of aSyn species. The presence of additional PTMs near the PTM of interest or interaction of aSyn species with other proteins could mask or interfere with the detection of specific aSyn species. Furthermore, aSyn within LBs exists in a complex environment where aSyn aggregates are not only modified at multiple residues but also interact with membranous organelles and a large number of proteins (Fig. 10a), mainly through the remaining flexible domains flanking the amyloid core. Furthermore, recent studies on aSyn fibrils obtained by amplifying brain-derived fibrils demonstrate that the C-terminal domain sequence comprising the residues S129 is highly structured and included in the core sequence of the fibrils (Fig. 10a). Finally, we have recently

demonstrated that aSyn astroglial synuclein accumulations are composed solely of aSyn proteins where the first 30 N-terminal amino acids and the last 35-40 C-terminal amino acids are absent. Such aSyn accumulations are not detected by any C-terminal targeting antibodies, including pS129 antibodies (unpublished results). Altogether, these observations suggest again that relying on only C-terminal targeting antibodies to detect, monitor, or quantify aSyn pathology may lead to underestimation or even misrepresentation of aSyn pathology.

Based on our findings and previous results, we propose a pipeline for systematic characterization and validation of pS129 antibodies before their application in PD research or their use in biomarker discovery and validation (Fig. 1a). We propose that all current and future antibodies against pS129 or other aSyn PTMs be screened first using aSyn protein standards containing the target PTM and proteins containing other PTMs that are known to co-occur with the target PTM. The antibodies that are insensitive to neighboring PTMs should then be screened using brain tissues and brain lysates from aSyn KO mice or rats. Antibodies that show specificity for the aSyn species/modification of interest should then be tested and optimized (e.g., dilutions) for the desired applications (e.g., studies on brain and peripheral tissues or studies on animal and cellular models of synucleinopathies). In these studies, the specificity of the antibodies should be further validated by including conditions where the antibody is pre-absorbed against a protein or peptide fragment(s) bearing the target sequence(s)/modification(s), or the antibody is omitted. Finally, it is essential to conduct a systematic analysis of the human and mouse proteome to determine which protein candidates are likely to cross-react with aSyn or aSyn-PTM-specific antibodies (Fig. 9). Knowing these proteins and whether they are present in the samples of interest (cells, tissues, or biological fluids) could help eliminate potential confounding factors and accelerate the development of specific tools and assays to detect and quantify aSyn species.

Our experience with antibodies has taught us that verifying the specificity of the antibodies saves not only time and money but also projects. Antibody batch-to-batch or lot-lot variability is more common than most people think or realize. This is because most antibodies are not rigorously characterized and validated by vendors before their distribution to research laboratories and that the validation data of new antibody batches are rarely made available. Most problems with antibodies are usually identified in research laboratories after significant time and resources have been wasted. During the past 5 years, we have had several experiences where we received lots of pS129 antibodies (from at least three different vendors) that did not exhibit the specificity and performance of the original lots. This contributes negatively to experimental reproducibility and could also lead to findings and controversies that distract and delay projects from coming to fruition. For example, recently, we conducted systematic characterization of 16 antibodies that were reported and used as aSyn oligomer-specific antibody[91]. We showed that none of these antibodies could distinguish between aSyn oligomers and fibrils, which raises questions about many of the claims made about the levels or role of aSyn oligomers in the pathogenesis of synucleinopathies based on these antibodies.

Therefore, to address many of the problems outlined above, we propose that researchers and reviewers should demand that (1) all new antibodies are thoroughly characterized and validated under physiologically relevant conditions and using the appropriate protein standards (Figs. 1a and S16); (2) the epitopes of all the antibodies should be disclosed, which will improve experimental design and enable more accurate interpretation of the results; (3) all new antibody batches are subjected to the same level of characterization and validation; (4) the resulting data are shared widely[92], and all validation data is included in publications or vendors' material data sheets; (5) all commercial antibodies are sold with the appropriate protein standards to allow the users to independently validate the antibodies in-house; and (6) the publication of negative results is encouraged.

Finally, funding agencies and publishers should incentivize and reward researchers who conduct studies and publish antibody characterization, validation, and reproducibility studies. Perhaps it is time to embrace the proposal of establishing certification programs for commercial antibodies[57].

METHODS

Reagents and antibodies
All the antibodies used in this study are described in Supplementary Fig. 3.

Expression and purification of aSyn
pT7-7 plasmids were used for the expression of recombinant human aSyn (WT, 1-133, 1-135) in *E. coli* and purified as previously described[93,94].

In vitro protein fibrillization
Lyophilized full-length WT aSyn protein was dissolved for in vitro studies in Tris buffer (50 mM Tris, 150 mM NaCl, pH 7.5, TBS) or phosphate-buffered saline (PBS, Invitrogen, Switzerland) for the cellular studies. The pH of the solution was adjusted to 7.2–7.5, and the protein was subsequently filtered through 0.22 μm polypropylene filters. Fibrils formation was induced by incubating the recombinant protein for 5 days under agitation (1000 rpm) on an orbital shaker at 37 °C. After incubation, the fibrils were fragmented by sonication (20 s, 20% amplitude, 1× pulse on, and 1× pulse off) and separated from the remaining soluble protein content (before and after sonication) by following a published protocol[94]. Sonicated aSyn fibrils were aliquoted and stored at −80 °C. As established by our laboratory[35,94,95], aSyn fibrils were systematically and thoroughly characterized by SDS-PAGE and Coomassie staining, Thioflavin T (ThT) aggregation assay, and their length distribution was estimated before and after sonication by electron microscopy. Each of these assays is detailed in the sections below.

Monomeric phosphorylated aSyn proteins
Phosphorylation of the recombinant (WT, 1-133, 1-135) and semisynthetic proteins (pY39, pS129, pY125, pS129) were produced and purified as described previously[28].

Nitration of aSyn fibrils
Post-fibrillization nitration of sonicated WT aSyn fibrils was induced with TNM (Sigma-Aldrich, Switzerland) following a published protocol[33]. Following nitration, the excess of TNM from nitrated fibrils was removed by washing steps in PBS using the 100-kDa MW-cut-off filters (Millipore, Switzerland) (13,000 rpm, 30 min, 4 °C). The success of post-fibrillization nitration was confirmed by LC-MS (ESI-LC-MS) and TEM.

Phosphorylation of nitrated fibrils by PLK3
Phosphorylation of nitrated aSyn fibrils was induced following a previously published protocol[13]. Briefly, WT nitrated aSyn fibrils were dissolved in the phosphorylation reaction buffer, and PLK3 (0.1 μg) was added and incubated at 30 °C without shaking. After 18 h of incubation, the reaction was analyzed by LC-MS.

Mass spectrometry analysis
Mass spectrometry analysis of proteins was performed by LC-MS on an LTQ system (Thermo Scientific, San Jose, CA) equipped with

an electrospray ion source and the MS instrument was operated in positive ion mode as previously described[94].

Characterization of aSyn fibrils by transmission electron microscopy (TEM)

To examine the ultrastructure of aSyn fibrils, negative staining electron microscope images were taken using Formvar/carbon-coated 200-mesh copper grids (Electron microscopy Sciences, Switzerland) as previously described[94]. Activated grids were loaded with 5 µl of sample for 30 s, washed three times with ultrapure water, and then negatively stained with 1% uranyl acetate for 1 min. Excess liquid was removed, and grids were allowed to air dry. Imaging was carried out on a Tecnai Spirit BioTWIN electron microscope operating at 80 kV acceleration voltage and equipped with a digital camera (FEI Eagle, FEI). A total of 3–5 images for each sample were chosen and the length of fibrils quantified (average 50–100 nm) using the Image J software (U.S. National Institutes of Health, MD, USA; RRID:SCR_001935).

Characterization of aSyn fibrils by ThT

The amyloid-like properties and the extent of fibrillization of aSyn fibrils were assessed by ThT fluorescence as explained previously[93,94]. The sonicated aSyn fibrils were resuspended in ThT solution (50 mM glycine pH 8.5, 10 µM ThT solution). ThT fluorescence was measured with a FLUOstar plate reader (BMG Labtech, Germany) at an excitation wavelength of 450 nm and an emission wavelength of 485 nm.

Characterization of aSyn fibrils by SDS-PAGE and Coomassie blue staining

The amount of soluble aSyn (monomers and oligomers) in the aSyn fibril solution was assessed before and after sonication after high-speed centrifugation by SDS-PAGE and Coomassie blue staining as previously described[94]. As sonication of aSyn fibrils can lead to the release of small amounts of monomers, only preparations with residual levels of aSyn monomers lower than 5% were used for the seeding in primary neurons[35].

Slot blot analysis

Monomeric or fibrillar aSyn proteins unmodified or subjected to different PTMs such as nitration, phosphorylation, or nitration/phosphorylation were loaded to a final concentration of 36 ng into the Slot Blot system (GE Healthcare, Switzerland). The system was assembled with a pre-wetting nitrocellulose membrane and two Whatman filters in PBS for 10 min, and each slot was washed with 200 µl PBS. Each protein (100 µl) was then loaded onto the membrane through the slots. The slot blot system was then disassembled, and the membrane was removed. The membrane was soaked in blocking buffer (Intercept blocking buffer, LicCOR, Germany)) at room temperature (RT) for 1 h before being incubated with the different primary pS129 antibodies at a dilution of 1/250. After 1 h, the membranes were extensively washed three times with PBS buffer containing 0.1% of Tween 20 (PBS-T) and then incubated at RT for 1 h with the respective secondary goat anti-mouse or anti-rabbit antibodies conjugated to Alexa fluor 680 or 800 dyes. The source and dilution of each antibody can be found in Supplementary Fig. 3. The membranes were then washed three times with PBS-T, and scanned on a LiCOR scanner (LiCOR, Germany). Afterwards, the same membranes were stained with SYN-1 or EGT 1-20 total aSyn antibodies. All the experiments were independently repeated three times.

ELISA

pS129 constructs (EPFL) and non-phosphorylated aSyn (Anaspec) were coated in a 96 well microplate (Nunc Maxisorp) at 0.1 µg/ml into a PBS buffer (Lonza) and incubated overnight at 4 °C. Tau441 (rPeptide) was included as a negative control protein. The microplates were washed once (PBS/0,05% Tween 20) followed by adding 300 µl of PBS/0.1% casein (Thermo Scientific) to block aspecific reactions. After 2 h at RT, the buffer was removed, and plates were dried overnight at RT. In the next step, the monoclonal pS129-aSyn antibodies (81A from BioLegend and MJF-R13 from Abcam) were diluted to 100 ng/ml into assay diluent (PBS/0.1% casein/0.2% Triton-X705) and 100 µl was added to the wells of the microplate plate followed by 1 h at RT. A blank was included where assay buffer was added without antibody. After another wash step, the antibodies were detected with 100 µl of a tracer antibody for respectively mouse (81A) and rabbit (MJF-R13) IgG species purchased to Jackson Immunoresearch (Goat anti-mouse H&L: Cat# 115-035-166; Donkey anti-rabbit: Cat#711-035-152) at a 5000 fold working dilution. After 5 wash steps, another 100 µl of a colorimetric substrate was added (generic substrate buffer Euroimmun ELISA test kits) and incubated for 0.5 h at RT, and the reaction was stopped by adding 50 µl of 1 M sulfuric acid. The OD 450–600 nm was further analyzed in a microplate reader (BMG Clariostar). All data points were tested in duplicate, and average values are reported in the table and figures.

Primary culture of hippocampal neurons and treatment with mouse aSyn fibrils

Primary hippocampal neurons were prepared from P0 pups of WT mice C57BL/6JRj (Janvier, France) or KO (C57BL/6J OlaHsd, Envigo, France) and cultured as previously described[35]. For high-content imaging and ICC, the neurons were seeded respectively in black, clear-bottomed, 96-well plates (Falcon, Switzerland) at a density of 200,000 cells/ml or onto coverslips (CS) (VWR, Switzerland) at a density of 250,000 cells/ml. For WB analysis, the neurons were plated on 6-well plates at a density of 300,000 cells/ml. All the plates were coated with poly-L-lysine 0.1% w/v in water (Brunschwig, Switzerland) before the plating. For the neuronal seeding model, the WT neurons after 6 days in culture (DIV 6) were treated with extracellular mouse aSyn PFFs at a final concentration of 70 nM and cultured for 14 or 21 days as previously described[32,34,35,68]. The mouse aSyn PFFs used in this study are from the same batch prepared and characterized in Mahul-Mellier et al.[32]. The E83Q aSyn PFFs used in this study are from the same batch prepared, characterized and used in Kumar et al.[37]. All procedures were approved by the Swiss Federal Veterinary Office (authorization numbers VD 3392 and VD 3694).

Stereotaxic injection of mouse aSyn fibrils

Male C57BL/6JRj mice (2–3 months of age, three animals per cage) were housed at 23°C, 40% humidity, with dark/light cycle of 12 h from 7 a.m. to 7 p.m. with access to standard laboratory rodent chow and water for in vivo experiments ad libitum. All animal experimentation procedures were approved by the Cantonal Veterinary Authorities (Vaud, Switzerland) and were performed according to the European Communities Council Directive of 24 November 1986 (86/609EEC). Every effort was taken to minimize the number of animals and their stress. Mice ($n = 12$) have been injected with 2.5 µl of mouse PFFs, prepared as previously described[94,96] in the right dorsal striatum (AP: 0.6, ML: 2.0, DV: −2.6). In detail, animals were anesthetized using a Ketamine/Xylazine cocktail. Once fully anesthetized, the animal was placed on the stereotaxic frame, head shaved, viscotears were applied to his eyes and liquid betadine solution was applied on the scalp before incision. Skull was cleaned from connective tissue with a scalpel and cleaned to highlight the bregma. Without damaging the dura mater, a small hole was drilled into the skull. Once in location, 2 µl of fibrils were injected in the right hemisphere at a flow rate of 0.4 µl/min. The needle was kept in place for 5 min and then slowly retracted and cleaned from blood to avoid clogging.

The animal was then sutured, betadine gel applied was to the wound and kept in a heated observation cage until fully awake.

Mammalian cell lines culture

HEK293 and HeLa cells were cultured at 95% air, and 5% $CO2$ in DMEM (for HEK293 and HeLa) supplemented with 10% fetal bovine serum (Invitrogen, Switzerland) and 1% of Penicillin/ Streptomycin (Invitrogen, Switzerland). The plasmid transfections were carried out by using the Effectene transfection reagent (Qiagen, Germany) according to the manufacturer's protocol. Mammalian cells were transfected with either the empty vector (pAAV) or human WT aSyn pAAV vector (Addgene plasmid # 36055; http://n2t.net/addgene:36055; RRID:Addgene_36055).

Sequential extraction of the soluble and insoluble fractions or subcellular fractionation of aSyn KO and WT primary neurons, brain homogenates, and mammalian cell lines

Preparation of soluble and insoluble fractions from aSyn KO and WT primary neurons and brain homogenates. At the indicated time, WT or aSyn KO primary cortical or hippocampal neurons (untreated or treated with WT aSyn mouse PFFs or with PBS as negative control)[32,34,35,68] or cortexes, striata, amygdala, and midbrains from aSyn KO mouse brains were lysed in 1% Triton X-100/ Tris-buffered saline (TBS) (50 mM Tris, 150 mM NaCl, pH 7.5) supplemented with protease inhibitor cocktail (Sigma-Aldrich, Switzerland), 1 mM phenylmethane sulfonyl fluoride (PMSF) (Sigma-Aldrich, Switzerland), and phosphatase inhibitor cocktails 2 and 3 (Sigma-Aldrich, Switzerland). Sequential biochemical fractionation of cell extracts was performed as described previously[32,35,68]. Cell lysates were sonicated using a fine probe [(0.5-s pulse at an amplitude of 20%, ten times (Sonic Vibra Cell, Blanc Labo, Switzerland], and then incubated on ice for 30 min before being centrifuged at $100,000 \times g$ for 30 min at 4 °C. The supernatant (soluble fraction) was collected. The pellet was washed in 1% Triton X-100/TBS and sonicated [(0.5-s pulse at an amplitude of 20%, ten times (Sonic Vibra Cell, Blanc Labo, Switzerland] before being centrifuged for 30 min at $100,000 \times g$. The supernatant was then discarded, and the pellet (insoluble fraction) was resuspended in 2% sodium dodecyl sulfate (SDS) diluted in TBS, pH 7.4 and finally sonicated using a fine probe [(0.5-s pulse at an amplitude of 20%, ten times (Sonic Vibra Cell, Blanc Labo, Switzerland].

Preparation of the total cell lysates from aSyn KO and WT primary neurons. Primary hippocampal or cortical neurons were lysed in 2% SDS/TBS supplemented with protease inhibitor cocktail, 1 mM PMSF, and phosphatase inhibitor cocktail 2 and 3 (Sigma-Aldrich, Switzerland) and boiled for 10 min as previously described[35].

Preparation of the nuclear, cytosolic and membrane fractions from aSyn KO and WT primary neurons and mammalian cell lines. Subcellular fractionation of the HEK and HeLa mammalian cells lines or the primary neurons was performed as previously described[97,98] and from Abcam protocol (https:// www.abcam.com/protocols/subcellular-fractionation-protocol) with minor modifications. Briefly, cells cultured in 10 cm culture plate (~5 million cells) were washed twice with ice-cold PBS and scraped with 500 μL fractionation buffer (20 mM HEPES at pH 7.4, 10 mM KCl, 2 mM $MgCl2$, 1 mM EDTA, 1 mM EGTA) supplemented extemporaneously with 1 mM of DTT, protease inhibitor cocktail (Sigma-Aldrich, Switzerland), 1 mM phenylmethane sulfonyl fluoride (PMSF) (Sigma-Aldrich, Switzerland), and phosphatase inhibitor cocktail 2 and 3 (Sigma-Aldrich, Switzerland). The cells in suspension were then incubated for 15 min on ice before being lysed mechanically using a Dounce homogenizer (with type B pestle). After 20 strokes, the cell homogenate was left 20 min on ice before being centrifuged at $720 \times g$ at 4 °C for 5 min. The

supernatant (cytosolic and membranes fractions), which contains the cytoplasm, membranes, and mitochondria, was then transferred into a fresh tube and kept on ice for 20 min.

The pellet corresponding to the nuclear fraction was washed with 500 μl fresh fractionation buffer to disperse the pellet. The resulting suspension was poured into a Dounce homogenizer (with type B pestle) and subjected to 20 strokes followed by centrifugation at $720 \times g$ at 4 °C for 10 min. The supernatant was discarded, and the final pellet (nuclear fraction) was resuspended in TBS supplemented with 0.1% SDS and sonicated briefly (3 s on ice at a power setting of 60%).

The cytosolic fraction was isolated from the membrane fraction after ultracentrifugation of the supernatant at $100,000 \times g$ at 4 °C for 1 h. The supernatant was collected and kept as the cytosolic fraction. The final pellet was washed by adding 400 μl of fractionation buffer, resuspended, and passed through Dounce homogenizer (with type B pestle-20 strokes) followed by a last ultracentrifugation step $100,000 \times g$ at 4 °C for 45 min. The pellet contains the membranes fraction that was resuspended in TBS (50 mM Tris-HCl- pH 7.6, 150 mM NaCl) supplemented with 0.1% SDS.

Tricine gels and WB analyses

The bicinchoninic acid (BCA) protein assay was performed to quantify the protein concentration in all the subcellular fractions (soluble, insoluble, nuclear, cytosolic, membrane and total cell extract) according to the supplier's protocol (Pierce, Thermofisher, Switzerland). Laemmli buffer 4× (10% SDS, 50% glycerol, 0.05% bromophenol blue, 1 M Tris-HCl pH 6.8 and 20% β-mercaptoethanol) was added to all the fractions. In all, 20–30 μg of proteins for each fraction were then separated on a 16% tricine gel[99]. Also, 0.5 μl of the PageRuler prestained protein ladder (10–180 kDa) from Thermofisher (Switzerland) was loaded for each gel. After 2 h of running, the gels were then transferred onto a nitrocellulose membrane (Amersham, Switzerland) with a semi-dry system (Bio-Rad, Switzerland), and immunoblotting was performed as previously described[32,35].

Immunocytochemistry

WT and aSyn KO primary hippocampal neurons untreated or treated with WT aSyn mouse[32] or E83Q human PFFs[37] were washed twice with PBS, fixed in 4% PFA for 20 min at RT, and then immunostained as previously described[32,35,95]. The antibodies used are indicated in the corresponding legend section of each figure. The source and dilution of each antibody can be found in Supplementary Fig. 3. The cells plated on CS were then examined with a confocal laser-scanning microscope (LSM 700, Carl Zeiss Microscopy, Germany) with a ×40 objective and analyzed using the Zen software (RRID:SCR_013672). The cells plated in black, clear-bottom, 96-well plates were imaged using the IN Cell Analyzer 2200 (with a ×10 objective). For each independent experiment, two wells were acquired per tested condition, and in each well, nine fields of view were imaged. Each experiment was reproduced at least three times independently.

Quantitative high-content wide-field cell imaging analyses (HCA)

After WT mouse aSyn PFFs treatment for 10 days, the primary hippocampal neurons plated in black, clear-bottom, 96-well plates (BD, Switzerland) were washed twice with PBS, fixed in 4% paraformaldehyde (PFA) for 20 min at RT and then immunostained as described above. Images were acquired using the Nikon ×10/ 0.45, Plan Apo, CFI/60 of the IN Cell Analyzer 2200 (GE Healthcare, Switzerland), a high-throughput imaging system equipped with a high-resolution 16-bits sCMOS camera (2048 × 2048 pixels), using a binning of 2 × 2. For each independent experiment, duplicated

wells were acquired per condition, and nine fields of view were imaged for each well. Each experiment was reproduced at least three times independently. Images were then analyzed using Cell profiler 3.0.0 software (RRID:SCR_007358) for identifying and quantifying the level of LB-like inclusions (stained with pS129 antibody) formed in neurons MAP2-positive cells, the number of neuronal cell bodies (co-stained with MAP2 staining and DAPI), or the number of neurites (stained with MAP2 staining). The pipeline of analysis is fully described in Mahul-Mellier et al.[35].

Immunochemistry on brain slides

Adult aSyn KO (C57BL/6J OlaHsd, Envigo) and Wild Type (C57BL6/J, Janvier labs) mouse fibrils-injected mice (3 months post-injection) were anesthetized using a solution containing 100 mg/Kg of Ketamine and 10 mg/Kg of xylazine. Once fully anesthetized, animals were perfused with PBS and then 4% PFA in PBS. Brains were rapidly extracted and left in PFA 4% at 4 °C for 24 h, after that, they were put in a 30% sucrose solution in PBS again at 4 °C for 24 h. Brains were then frozen in isopentane, stored at −80 °C, and subsequently cut into 50 µm-thick coronal slides with seriality of one every four sections and stored in a PBS-azide 0.1% solution at 4 °C until further processing. Free-floating coronal slices from 5 different animals were rinsed 3 times for 5 min in PBS and then incubated 10 min in a 10% hydrogen peroxide solution in PBS, then washed again twice for 5 min in PBS, left in a 2.5% Normal Horse Serum blocking solution for 30 min (ImmPRESS, Vector laboratories, Germany) and then incubated overnight at 4 °C shaking with primary antibodies (Supplementary Fig. 3) diluted in blocking solution. The following day, slices were rinsed 3 times in PBS and then incubated 1 h at RT with either ImmPRESS® HRP Horse Anti-Mouse IgG Polymer (Vector Laboratories Cat# MP-7402, RRID:AB_2336528) or ImmPRESS® HRP Horse Anti-Rabbit IgG Polymer (Vector Laboratories Cat# MP-7401, RRID:AB_2336529), according to primary antibody's host species. After incubation, slices were rinsed again 4 times for 5 min in PBS and revealed using a DAB substrate kit (Vector Laboratories Cat# SK-4100, RRID:AB_2336382). Stained slices (at least 5 per region) were then mounted on gelatinized slides, coverslipped and imaged at ×20 using an VS120-SL Olympus slide scanner microscope (Olympus, Germany). All procedures were approved by the Swiss Federal Veterinary Office (authorization number VD2067).

Quantification of pS129 pathology in PFF-injected WT mice

Quantification of pS129 stained slices was carried out using Qupath[100]. Briefly, Brain regions have been outlined as annotations for each slice and positive pixel count was evaluated with a downsample factor of 1, Gaussian sigma of 0.3, negative threshold of 100 and with a DAB-positive threshold based on the minimum intensity value considered as positive. Finally, the value for each mouse in each region is obtained by addition of the area value of all the brain slices of each mouse divided by the addition of total ROI area. Values were then expressed as percentages of positive area of total ROI.

Imaris processing

Nuclear and the "nuclear-like" pS129-aSyn aggregates segmentation and visualization were performed using Imaris version 9.9.1.

The nuclear signal was segmented as 3D surfaces using a 3D Gaussian smoothing with sigma=0.5 µm and a manual absolute threshold value of 12. Only the largest surface, corresponding to the nucleus, was kept by applying a size filter, keeping objects only when above 10,000 voxels. pS129-aSyn aggregates were segmented as 3D surfaces using a smoothing of sigma = 0.156 µm and a local background subtraction with the largest sphere diameter of 0.586 µm followed by a manual threshold of 12.

3D animations showing the interior of the nuclear surface clearly show that the "nuclear-like" pS129-aSyn aggregates are found within the nuclear volume. Imaris files are available upon request.

Identification of putative antibody cross-reaction candidates

All human and mouse phosphorylation sites annotated in Uniprot were retrieved as full-text entries using the https://www.uniprot.org server on June 15, 2020 by entering the following terms in the search box for UniProtKB: (annotation:(type:mod_res phosphoserine) OR annotation:(type:mod_res phosphotyrosine)) (organism:"Homo sapiens (Human) [9606]" OR organism:"Mus musculus (Mouse) [10090]") AND reviewed:yes.

A perl script was used to parse the entries, extract protein sequence fragments of 13 residues centered on each documented annotated phosphorylation site and compare them to the six human aSyn fragments shown in Fig. 9a. Residues immediately preceding and following the phosphorylation site were requested to be perfect matches. For all protein fragments retrieved from Uniprot satisfying this condition (Supplementary Figs. 14 and 15), we computed the number of exact and highly similar matches to the six aSyn fragments and the length of the longest continuous stretch of perfect or similar matches encompassing the phosphorylation site. High similarity criteria were defined as a PAM120 matrix score of two matching residues strictly greater than 1. This would include, for example, Glu ≅ Gln (score = 2) and Tyr ≅ Phe (score = 4) but exclude Ile ≠ Leu (score = 1) and Ile ≠ Phe (score = 0).

For each of the six aSyn fragments, hits were sorted by the number of continuous exact match stretch, then the number of continuous exact + similar match stretch, then the number of exact matches, then the number of similar matches, then the molecular weight.

Subcellular location annotations were retrieved by parsing the "CC -!- SUBCELLULAR LOCATION:" fields of the corresponding Uniprot entries.

Three online databases, i.e., The Human Protein Atlas, https://www.proteinatlas.org/; Proteomics DB, https://www.proteomicsdb.org/proteomicsdb/; and CSF proteome resource, https://proteomics.uib.no/csf-pr/ were used to evaluate whether the proteins were previously identified in human plasma or CSF.

REFERENCES

1. Anderson, J. P. et al. Phosphorylation of Ser-129 is the dominant pathological modification of alpha-synuclein in familial and sporadic Lewy body disease. *J. Biol. Chem.* **281**, 29739–29752 (2006).
2. Walker, D. G. et al. Changes in properties of serine 129 phosphorylated α-synuclein with progression of Lewy-type histopathology in human brains. *Exp. Neurol.* **240**, 190–204 (2013).
3. Kellie, J. F. et al. Quantitative measurement of intact alpha-synuclein proteoforms from post-mortem control and Parkinson's disease brain tissue by intact protein mass spectrometry. *Sci. Rep.* **4**, 5797 (2014).
4. Delic, V. et al. Sensitivity and specificity of phospho-Ser129 α-synuclein monoclonal antibodies. *J. Comp. Neurol.* **526**, 1978–1990 (2018).
5. Fayyad, M. et al. Generation of monoclonal antibodies against phosphorylated α-Synuclein at serine 129: research tools for synucleinopathies. *Neurosci. Lett.* **725**, 134899 (2020).

6. Sacino, A. N. et al. Amyloidogenic α-synuclein seeds do not invariably induce rapid, widespread pathology in mice. Acta Neuropathol. 127, 645–665 (2014).

7. Uchihara, T. & Giasson, B. I. Propagation of alpha-synuclein pathology: hypotheses, discoveries, and yet unresolved questions from experimental and human brain studies. Acta Neuropathol. 131, 49–73 (2016).

8. Killinger, B. A. et al. Distribution of phosphorylated alpha-synuclein in non-diseased brain implicates olfactory bulb mitral cells in synucleinopathy pathogenesis. Preprint at bioRxiv https://doi.org/10.1101/2021.12.22.473905 (2021).

9. Rutherford, N. J., Brooks, M. & Giasson, B. I. Novel antibodies to phosphorylated α-synuclein serine 129 and NFL serine 473 demonstrate the close molecular homology of these epitopes. Acta Neuropathol. Commun. 4, 80 (2016).

10. Mbefo, M. K. et al. Parkinson disease mutant E46K enhances α-synuclein phosphorylation in mammalian cell lines, in yeast, and in vivo. J. Biol. Chem. 290, 9412–9427 (2015).

11. Arlinghaus, R., Iba, M., Masliah, E., Cookson, M. R. & Landeck, N. Specific detection of endogenous s129 phosphorylated α-synuclein in tissue using proximity ligation assay. Preprint at bioRxiv https://doi.org/10.1101/2021.09.28.461511 (2021).

12. Ellis, C. E., Schwartzberg, P. L., Grider, T. L., Fink, D. W. & Nussbaum, R. L. alpha-synuclein is phosphorylated by members of the Src family of protein-tyrosine kinases. J. Biol. Chem. 276, 3879–3884 (2001).

13. Duda, J. E. et al. Widespread nitration of pathological inclusions in neurodegenerative synucleinopathies. Am. J. Pathol. 157, 1439–1445 (2000).

14. Bhattacharjee, P. et al. Mass spectrometric analysis of Lewy body-enriched α-synuclein in Parkinson's disease. J. Proteome Res. 18, 2109–2120 (2019).

15. Ohrfelt, A. et al. Identification of novel α-synuclein isoforms in human brain tissue by using an online nanoLC-ESI-FTICR-MS method. Neurochem. Res. 36, 2029–2042 (2011).

16. Kiely, A. P. et al. α-Synucleinopathy associated with G51D SNCA mutation: a link between Parkinson's disease and multiple system atrophy? Acta Neuropathol. 125, 753–769 (2013).

17. Baba, M. et al. Aggregation of alpha-synuclein in Lewy bodies of sporadic Parkinson's disease and dementia with Lewy bodies. Am. J. Pathol. 152, 879–884 (1998).

18. Killinger, B. A. et al. In situ proximity labeling identifies Lewy pathology molecular interactions in the human brain. Proc. Natl Acad. Sci. USA 119, e2114405119 (2022).

19. Moors, T. E. et al. The subcellular arrangement of alpha-synuclein proteoforms in the Parkinson's disease brain as revealed by multicolor STED microscopy. Acta Neuropathol. 142, 423–448 (2021).

20. Prasad, K., Beach, T. G., Hedreen, J. & Richfield, E. K. Critical role of truncated alpha-synuclein and aggregates in Parkinson's disease and incidental Lewy body disease. Brain Pathol. 22, 811–825 (2012).

21. Waxman, E. A., Duda, J. E. & Giasson, B. I. Characterization of antibodies that selectively detect alpha-synuclein in pathological inclusions. Acta Neuropathol. 116, 37–46 (2008).

22. Killinger, B. A. et al. The vermiform appendix impacts the risk of developing Parkinson's disease. Sci. Transl. Med. https://doi.org/10.1126/scitranslmed.aar5280 (2018).

23. Fayyad, M. et al. Investigating the presence of doubly phosphorylated α-synuclein at tyrosine 125 and serine 129 in idiopathic Lewy body diseases. Brain Pathol. 30, 831–843 (2020).

24. Muntane, G., Ferrer, I. & Martinez-Vicente, M. alpha-synuclein phosphorylation and truncation are normal events in the adult human brain. Neuroscience 200, 106–119 (2012).

25. Sano, K. et al. Tyrosine 136 phosphorylation of α-synuclein aggregates in the Lewy body dementia brain: involvement of serine 129 phosphorylation by casein kinase 2. Acta Neuropathol. Commun. 9, 182 (2021).

26. Lassozé, S. et al. Comparison of commercially available antibodies for the detection of phosphorylated alpha-synuclein in primary culture of ENS. Neurogastroenterol. Motil. https://doi.org/10.1111/nmo.14354 (2022).

27. Burai, R., Ait-Bouziad, N., Chiki, A. & Lashuel, H. A. Elucidating the role of site-specific nitration of alpha-synuclein in the pathogenesis of Parkinson's disease via protein semisynthesis and mutagenesis. J. Am. Chem. Soc. 137, 5041–5052 (2015).

28. Fauvet, B. & Lashuel, H. A. Semisynthesis and enzymatic preparation of post-translationally modified alpha-synuclein. Methods Mol. Biol. 1345, 3–20 (2016).

29. Hejjaoui, M. et al. Elucidating the role of C-terminal post-translational modifications using protein semisynthesis strategies: alpha-synuclein phosphorylation at tyrosine 125. J. Am. Chem. Soc. 134, 5196–5210 (2012).

30. Sorrentino, Z. A. et al. Physiological carboxy-truncation of alpha-synuclein potentiates the prion-like formation of pathological inclusions. J. Biol. Chem. https://doi.org/10.1074/jbc.RA118.005603 (2018).

31. Pieri, L. et al. Cellular response of human neuroblastoma cells to alpha-synuclein fibrils, the main constituent of Lewy bodies. Biochim. Biophys. Acta 1860, 8–19 (2016).

32. Mahul-Mellier, A.-L. et al. The making of a Lewy body: the role of α-synuclein post-fibrillization modifications in regulating the formation and the maturation of pathological inclusions. Preprint at bioRxiv https://doi.org/10.1101/500058 (2018).

33. Radi, R. Nitric oxide, oxidants, and protein tyrosine nitration. Proc. Natl Acad. Sci. USA 101, 4003–4008 (2004).

34. Volpicelli-Daley, L. A. et al. Exogenous alpha-synuclein fibrils induce Lewy body pathology leading to synaptic dysfunction and neuron death. Neuron. 72, 57–71 (2011).

35. Mahul-Mellier, A. L. et al. The process of Lewy body formation, rather than simply α-synuclein fibrillization, is one of the major drivers of neurodegeneration. Proc. Natl Acad. Sci. USA 117, 4971–4982 (2020).

36. Haj-Yahya, M. et al. Synthetic polyubiquitinated α-Synuclein reveals important insights into the roles of the ubiquitin chain in regulating its pathophysiology. Proc. Natl Acad. Sci. USA 110, 17726–17731 (2013).

37. Kumar, S. T. et al. A NAC domain mutation (E83Q) unlocks the pathogenicity of human alpha-synuclein and recapitulates its pathological diversity. Sci. Adv. 8, eabn0044 (2022).

38. Kapasi, A. et al. A novel SNCA E83Q mutation in a case of dementia with Lewy bodies and atypical frontotemporal lobar degeneration. Neuropathology 40, 620–626 (2020).

39. Fujiwara, H. et al. alpha-Synuclein is phosphorylated in synucleinopathy lesions. Nat. Cell Biol. 4, 160–164 (2002).

40. Katsuse, O., Iseki, E., Marui, W. & Kosaka, K. Developmental stages of cortical Lewy bodies and their relation to axonal transport blockage in brains of patients with dementia with Lewy bodies. J. Neurol. Sci. 211, 29–35 (2003).

41. Gai, W. P., Power, J. H., Blumbergs, P. C., Culvenor, J. G. & Jensen, P. H. Alpha-synuclein immunoisolation of glial inclusions from multiple system atrophy brain tissue reveals multiprotein components. J. Neurochemistry 73, 2093–2100 (1999).

42. Gai, W. P. et al. In situ and in vitro study of colocalization and segregation of alpha-synuclein, ubiquitin, and lipids in Lewy bodies. Exp. Neurol. 166, 324–333 (2000).

43. Irizarry, M. C. et al. Nigral and cortical Lewy bodies and dystrophic nigral neurites in Parkinson's disease and cortical Lewy body disease contain a-synuclein immunoreactivity. J. Neuropathol. Exp. Neurol. 57, 334–337 (1998).

44. Harding, A. J. & Halliday, G. M. Cortical Lewy body pathology in the diagnosis of dementia. Acta Neuropathol. 102, 355–363 (2001).

45. Spillantini, M. G., Crowther, R. A., Jakes, R., Hasegawa, M. & Goedert, M. alpha-Synuclein in filamentous inclusions of Lewy bodies from Parkinson's disease and dementia with lewy bodies. Proc. Natl Acad. Sci. USA 95, 6469–6473 (1998).

46. Huang, Y. & Halliday, G. Can we clinically diagnose dementia with Lewy bodies yet? Transl. Neurodegener. 2, 4 (2013).

47. Kuusisto, E., Parkkinen, L. & Alafuzoff, I. Morphogenesis of Lewy bodies: dissimilar incorporation of alpha-synuclein, ubiquitin, and p62. J. Neuropathol. Exp. Neurol. 62, 1241–1253 (2003).

48. Grassi, D., Diaz-Perez, N., Volpicelli-Daley, L. A. & Lasmezas, C. I. Palpha-syn* mitotoxicity is linked to MAPK activation and involves tau phosphorylation and aggregation at the mitochondria. Neurobiol. Dis. 124, 248–262 (2019).

49. Grassi, D. et al. Identification of a highly neurotoxic alpha-synuclein species inducing mitochondrial damage and mitophagy in Parkinson's disease. Proc. Natl Acad. Sci. USA 115, E2634–E2643 (2018).

50. Schell, H., Hasegawa, T., Neumann, M. & Kahle, P. J. Nuclear and neuritic distribution of serine-129 phosphorylated alpha-synuclein in transgenic mice. Neuroscience 160, 796–804 (2009).

51. Wakamatsu, M. et al. Accumulation of phosphorylated alpha-synuclein in dopaminergic neurons of transgenic mice that express human alpha-synuclein. J. Neurosci. Res. 85, 1819–1825 (2007).

52. Villar-Piqué, A. et al. Environmental and genetic factors support the dissociation between α-synuclein aggregation and toxicity. Proc. Natl Acad. Sci. USA 113, E6506–E6515 (2016).

53. Pinho, R. et al. Nuclear localization and phosphorylation modulate pathological effects of alpha-synuclein. Hum. Mol. Genet. 28, 31–50 (2019).

54. Davidi, D. et al. α-Synuclein translocates to the nucleus to activate retinoic-acid-dependent gene transcription. iScience 23, 100910 (2020).

55. Elfarrash, S. et al. Polo-like kinase 2 inhibition reduces serine-129 phosphorylation of physiological nuclear alpha-synuclein but not of the aggregated alpha-synuclein. PLoS ONE 16, e0252635 (2021).

56. Li, B. et al. Cryo-EM of full-length α-synuclein reveals fibril polymorphs with a common structural kernel. Nat. Commun. 9, 3609 (2018).

57. Baker, M. When antibodies mislead: the quest for validation. Nature 585, 313–314 (2020).

58. Voskuil, J. L. A. et al. The Antibody Society's antibody validation webinar series. MAbs 12, 1794421 (2020).

59. Alafuzoff, I. et al. Staging/typing of Lewy body related alpha-synuclein pathology: a study of the BrainNet Europe Consortium. *Acta Neuropathol.* **117**, 635–652 (2009).

60. Braak, H. et al. Staging of brain pathology related to sporadic Parkinson's disease. *Neurobiol. Aging* **24**, 197–211 (2003).

61. Braak, H., Sastre, M. & Del Tredici, K. Development of alpha-synuclein immunoreactive astrocytes in the forebrain parallels stages of intraneuronal pathology in sporadic Parkinson's disease. *Acta Neuropathol.* **114**, 231–241 (2007).

62. Luk, K. C. et al. Pathological α-synuclein transmission initiates Parkinson-like neurodegeneration in nontransgenic mice. *Science* **338**, 949–953 (2012).

63. Peelaerts, W., Bousset, L., Baekelandt, V. & Melki, R. a-Synuclein strains and seeding in Parkinson's disease, incidental Lewy body disease, dementia with Lewy bodies and multiple system atrophy: similarities and differences. *Cell Tissue Res.* https://doi.org/10.1007/s00441-018-2839-5 (2018).

64. Peelaerts, W. et al. α-Synuclein strains cause distinct synucleinopathies after local and systemic administration. *Nature* **522**, 340–344 (2015).

65. Paumier, K. L. et al. Intrastriatal injection of pre-formed mouse alpha-synuclein fibrils into rats triggers alpha-synuclein pathology and bilateral nigrostriatal degeneration. *Neurobiol. Dis.* **82**, 185–199 (2015).

66. Luk, K. C. et al. Exogenous alpha-synuclein fibrils seed the formation of Lewy body-like intracellular inclusions in cultured cells. *Proc. Natl Acad. Sci. USA* **106**, 20051–20056 (2009).

67. Tanik, S. A., Schultheiss, C. E., Volpicelli-Daley, L. A., Brunden, K. R. & Lee, V. M. Lewy body-like alpha-synuclein aggregates resist degradation and impair macroautophagy. *J. Biol. Chem.* **288**, 15194–15210 (2013).

68. Volpicelli-Daley, L. A., Luk, K. C. & Lee, V. M. Addition of exogenous alpha-synuclein preformed fibrils to primary neuronal cultures to seed recruitment of endogenous alpha-synuclein to Lewy body and Lewy neurite-like aggregates. *Nat. Protoc.* **9**, 2135–2146 (2014).

69. Zhao, Q. et al. Neuroprotective effects of lithium on a chronic MPTP mouse model of Parkinson's disease via regulation of α-synuclein methylation. *Mol. Med. Rep.* **19**, 4989–4997 (2019).

70. Liu, H. F. et al. LRRK2 R1441G mice are more liable to dopamine depletion and locomotor inactivity. *Ann. Clin. Transl. Neurol.* **1**, 199–208 (2014).

71. Nishie, M. et al. Accumulation of phosphorylated alpha-synuclein in the brain and peripheral ganglia of patients with multiple system atrophy. *Acta Neuropathol.* **107**, 292–298 (2004).

72. Lue, L. F. et al. Biochemical increase in phosphorylated alpha-synuclein precedes histopathology of Lewy-type synucleinopathies. *Brain Pathol.* **22**, 745–756 (2012).

73. Henderson, M. X. et al. LRRK2 inhibition does not impart protection from α-synuclein pathology and neuron death in non-transgenic mice. *Acta Neuropathol. Commun.* **7**, 28 (2019).

74. Gentzel, R. C. et al. Intracranial administration of alpha-synuclein fibrils in A30P-synuclein transgenic mice causes robust synucleinopathy and microglial induction. *Neurobiol. Aging* **106**, 12–25 (2021).

75. Zhang, J., Li, X. & Li, J. D. The roles of post-translational modifications on alpha-synuclein in the pathogenesis of Parkinson's diseases. *Front. Neurosci.* **13**, 381 (2019).

76. Wakabayashi, K. et al. The Lewy body in Parkinson's disease and related neurodegenerative disorders. *Mol. Neurobiol.* **47**, 495–508 (2013).

77. Petricca, L. et al. Comparative analysis of total alpha-synuclein (αSYN) immunoassays reveals that they do not capture the diversity of modified αSYN proteoforms. *J. Parkinsons Dis.* **12**, 1449–1462 (2022).

78. Sorrentino, Z. A., Giasson, B. I. & Chakrabarty, P. α-Synuclein and astrocytes: tracing the pathways from homeostasis to neurodegeneration in Lewy body disease. *Acta Neuropathol.* **138**, 1–21 (2019).

79. Yokota, O. et al. NACP/alpha-synuclein immunoreactivity in diffuse neurofibrillary tangles with calcification (DNTC). *Acta Neuropathol.* **104**, 333–341 (2002).

80. Terada, S. et al. Glial involvement in diffuse Lewy body disease. *Acta Neuropathol.* **105**, 163–169 (2003).

81. Takeda, A. et al. C-terminal alpha-synuclein immunoreactivity in structures other than Lewy bodies in neurodegenerative disorders. *Acta Neuropathol.* **99**, 296–304 (2000).

82. Henderson, M. X. et al. Glucocerebrosidase activity modulates neuronal susceptibility to pathological α-synuclein insult. *Neuron* **105**, 822.e7–836.e7 (2020).

83. Goers, J. et al. Nuclear localization of alpha-synuclein and its interaction with histones. *Biochemistry* **42**, 8465–8471 (2003).

84. Pouclet, H. et al. A comparison between colonic submucosa and mucosa to detect Lewy pathology in Parkinson's disease. *Neurogastroenterol. Motil.* **24**, e202–e205 (2012).

85. Doppler, K. et al. Cutaneous neuropathy in Parkinson's disease: a window into brain pathology. *Acta Neuropathol.* **128**, 99–109 (2014).

86. Norman, M., Gilboa, T. & Walt, D. R. High-sensitivity single molecule array assays for pathological isoforms in Parkinson's disease. *Clin. Chem.* **68**, 431–440 (2022).

87. Lin, C. H. et al. Plasma pS129-alpha-synuclein is a surrogate biofluid marker of motor severity and progression in Parkinson's disease. *J. Clin. Med.* https://doi.org/10.3390/jcm8101601 (2019).

88. Cariulo, C. et al. Phospho-S129 alpha-synuclein is present in human plasma but not in cerebrospinal fluid as determined by an ultrasensitive immunoassay. *Front. Neurosci.* **13**, 889 (2019).

89. Preterre, C. et al. Optimizing western blots for the detection of endogenous alpha-synuclein in the enteric nervous system. *J. Parkinsons Dis.* **5**, 765–772 (2015).

90. Stephens, A. D. et al. Extent of N-terminus exposure of monomeric alpha-synuclein determines its aggregation propensity. *Nat. Commun.* **11**, 2820 (2020).

91. Kumar, S. T. et al. How specific are the conformation-specific α-synuclein antibodies? Characterization and validation of 16 α-synuclein conformation-specific antibodies using well-characterized preparations of α-synuclein monomers, fibrils and oligomers with distinct structures and morphology. *Neurobiol. Dis.* **146**, 105086 (2020).

92. Voskuil, J. L. The challenges with the validation of research antibodies. *F1000Res* **6**, 161 (2017).

93. Fauvet, B. et al. α-Synuclein in central nervous system and from erythrocytes, mammalian cells, and *Escherichia coli* exists predominantly as disordered monomer. *J. Biol. Chem.* **287**, 15345–15364 (2012).

94. Kumar, S. T., Donzelli, S., Chiki, A., Syed, M. M. K. & Lashuel, H. A. A simple, versatile and robust centrifugation-based filtration protocol for the isolation and quantification of α-synuclein monomers, oligomers and fibrils: towards improving experimental reproducibility in α-synuclein research. *J. Neurochemistry* **153**, 103–119 (2020).

95. Mahul-Mellier, A. L. et al. Fibril growth and seeding capacity play key roles in α-synuclein-mediated apoptotic cell death. *Cell Death Differ.* **22**, 2107–2122 (2015).

96. Burtscher, J. et al. Chronic corticosterone aggravates behavioral and neuronal symptomatology in a mouse model of alpha-synuclein pathology. *Neurobiol. Aging* **83**, 11–20 (2019).

97. Borin, M. et al. Rac1 activation links tau hyperphosphorylation and Aβ dysmetabolism in Alzheimer's disease. *Acta Neuropathol. Commun.* **6**, 61 (2018).

98. Yu, Z., Huang, Z. & Lung, M. L. Subcellular fractionation of cultured human cell lines. *BioProtoc.* **3**, e754 (2013).

99. Schägger, H. Tricine-SDS-PAGE. *Nat. Protoc.* **1**, 16–22 (2006).

100. Bankhead, P. et al. QuPath: open source software for digital pathology image analysis. *Sci. Rep.* https://doi.org/10.1038/s41598-017-17204-5 (2017).

101. Guerrero-Ferreira, R. et al. Two new polymorphic structures of human full-length alpha-synuclein fibrils solved by cryo-electron microscopy. *Elife* **8**, e48907 (2019).

102. Zhao, K. et al. Parkinson's disease-related phosphorylation at Tyr39 rearranges α-synuclein amyloid fibril structure revealed by cryo-EM. *Proc. Natl Acad. Sci. USA* **117**, 20305–20315 (2020).

103. Schweighauser, M. et al. Structures of α-synuclein filaments from multiple system atrophy. *Nature* **585**, 464–469 (2020).

ACKNOWLEDGEMENTS

AUTHOR CONTRIBUTIONS

Conceptualization: H.A.L. Design of the work: H.A.L. Methodology: A.-L.M.-M., S.N., R.N.H., Y.J., M.F.A., S.D., S.M.G., R.B., J.R., M.B., P.M., E.S., C.I., N.G., A.C. Investigation and acquisition: H.A.L., A.-L.M.-M., S.N., R.N.H., Y.J., M.F.A., S.D., S.M.G., R.B., J.R., M.B., P.M., E.S., C.I., N.G., A.C. Data curation: H.A.L., A.-L.M.-M., S.N., R.N.H., Y.J., M.F.A., S.D., S.M.G., R.B., J.R., M.B., P.M., E.S., C.I., N.G., A.C. Formal analysis and interpretation of the data: H.A.L., A.-L.M.-M., S.N., R.N.H., M.F.A., S.D., S.M.G., R.B., P.M., E.S., C.I., N.G. Validation: H.A.L., A.-L.M.-M., S.N., R.N.H., M.F.A., S.D., S.M.G., R.B., P.M., E.S., C.I, N.G. Visualization: H.A.L., A.-L.M.-M., S.N., R.N.H., Y.J., M.F.A., S.D., S.M.G., R.B., J.R., M.B., P.M., A.S., E.S., C.I., N.G., A.C. Software: P.M., E.S., C.I., N.G. Writing—original draft: H.A.L. Writing—review and editing and revision: H.A.L., A.-L.M.-M., S.N., P.M. Final approval of the completed version: H.A.L., A.-L.M.-M., S.N. Funding acquisition: H.A.L. Project administration: H.A.L. Resources: H.A.L. Supervision and accountability for all aspects of the work in ensuring that questions related to the accuracy and integrity of any part of the work are appropriately investigated and resolved: H.A.L.

COMPETING INTERESTS

ADDITIONAL INFORMATION

Supplementary information The online version contains supplementary material available at https://doi.org/10.1038/s41531-022-00388-7.

Correspondence and requests for materials should be addressed to Hilal A. Lashuel.

Reprints and permission information is available at http://www.nature.com/reprints

Publisher's note Springer Nature remains neutral with regard to jurisdictional claims in published maps and institutional affiliations.